Rapp. SMHI (Ex1)

SMHI

Reports Meteorology and Climatology

No 105 August, 2004

SVERIGES METEOROLOGISKA OCH HYDROLOGISKA INSTITUT
2004 -08- 17
BIBLIOTEKET

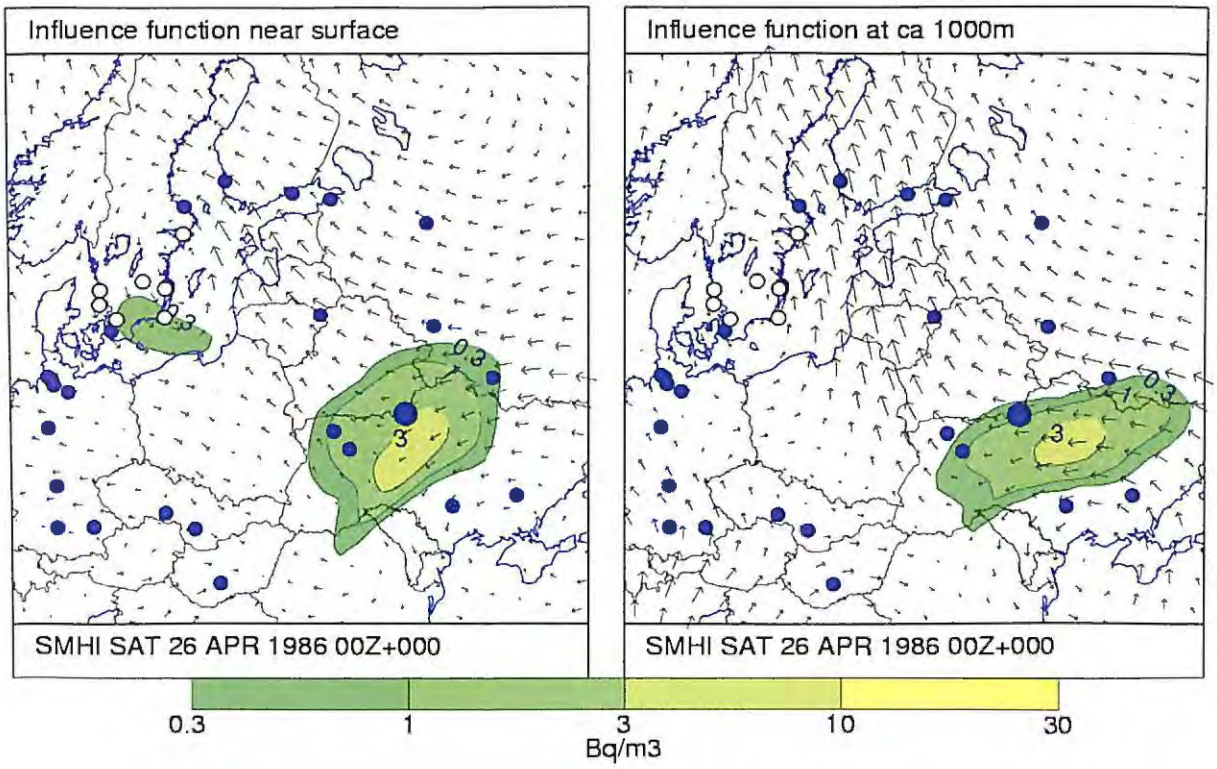

Extended back-trajectories by means of adjoint equations

Lennart Robertson

Rapporten är finansierad av SSI

RMK
No 105, August 2004

Extended back-trajectories by means of adjoint equations

Lennart Robertson

Report Summary / Rapportsammanfattning

Issuing Agency/Utgivare	Report number/Publikation
Swedish Meteorological and Hydrological Institute S-601 76 NORRKÖPING Sweden	RMK No. 105
	Report date/Utgivningsdatum August 2004

Author (s)/Författare

Lennart Robertson

Title (and Subtitle/Titel

Extended back-trajectories by means of adjoint equations

Abstract/Sammandrag

Back-trajectory models are examples of the most simple adjoint models used for tracing of important source regions attributed to measured tracers. These models do, however, suffer from oversimplification of the transport-diffusion processes in the atmosphere. By utilizing adjoint equations in a 3D transport-diffusion model several advantages could be achieved, all transport mechanisms are included and the response at receptor points could more properly mimic the sampled time-period of the measurements. In this paper the concept of adjoint equations is described, the similarity between back-trajectories and the adjoint technique is demonstrated, and options of using the adjoint technique for guidance of emission sources are explored. To illustrate the possibilities four different events are examined, the Chernobyl accident, the ETEX I exercise, the Algeciras accident and an event with heavy smoke noticed in Scandinavia. Finally, a suggestion for an operational setup is discussed.

Key words/sök-, nyckelord

Atmospheric dispersion, MATCH model, Adjoint equations, Trajectories.

Supplementary notes/Tillägg	Number of pages/Antal sidor	Language/Språk
The report is financed by The Swedish Radiation Protection Agency, SSI, contract SSI P 1240.00.	37	English

ISSN and title/ISSN och titel

0347-2116 SMHI Reports Meteorology Climatology

Report available from/Rapporten kan köpas från:

SMHI
S-601 76 NORRKÖPING
Sweden

Contents

1 Introduction

The back-trajectory is an easy but powerful tool for assessing possible source origin of a measured trace species. In an important study on the Chernobyl accident Persson et al. (1987) used this approach to estimate the amount released from the rampaged nuclear power station.

However, back-trajectories suffer from oversimplifications of the transport-diffusion process by entirely omitting diffusion. Moreover, the nature of trajectories is to follow a single air parcel implying a very short response at the receptor point. These deficiencies are not always in mind when interpreting backward trajectories. However, the adjoint technique applied to a 3D dispersion model would inherently include more of the transport mechanisms and allow for longer response times at the receptor.

Using adjoint equations was first described by Kontarev (1980) and Marchuk and Penenko (1980) for complex dynamical systems. Applications for environmental problems were outlined by Marchuk (1986) and Uliasz (1987), basicly discussing influence functions in the framework of a receptor oriented approach.

The adjoint technique is now found in different disciplines such as numerical weather prediction with some early work by Talagrand and Courtier (1987), Lorenc (1988) and Derber (1989). Vast amount of literature exist on this subject, lately various aspects on variational methods have been published by Le Dimet et *al.* (2002), Park and Zupanski (2003), Purser et *al.* (2003), Mu and Wang (2003). Adjoint methods have been discussed in oceanography by Ghil and Malanotte-Rizzoli (1991) and Sirkes and Tziperman (2001). Chardigny et *al.* (1996) and Shen and Kuo (1999) discussed calibration of hydrological models including remote sensing by means of adjoint methods, and Van den Berghe (1993) presented variational techniques for mapping pollutants in lakes.

In air pollution modeling early work was done by Marchuk (1986) and Uliasz (1987) and lately Pudykiewicz (1998) and Wotawa et *al.* (2003) presented work in connection to the Comprehensive Test Ban Treaty (CTBT), where the concept of "fields of regard" comes close to the objective of this paper. Data assimilation in dispersion models have been discussed by Robertson and Persson (1993), Robertson and Langner (1998), Tanguay and Polavarapu (1999), Houweling et *al.* (1999), Menut (2003) and Konstadinos and Robertson (2003). The extension of data assimilation by including complex chemistry have been demonstrated by Uliasz and Pielke (1991), Elbern and Schmidt (1999), Daescu et *al.* (2003a,2003b) and Schmidt and Martin (2003).

In this paper we will explore the options of using adjoint modeling in contrast to traditional back-trajectory models, very much in line with the receptor oriented approach discussed by Uliasz and Pielke (1991), Pudykiewicz (1998) and Rivin and Voronina (2001). The purpose is thus not to perform data assimilation as such but to explore the use of observations in terms of possible source regions. Special attention is paid to the impact from the temporal resolution in measured values.

The basis for this work is the MATCH model (Robertson et *al.*, 1999) into which adjoint equations have been implemented.

In Section 2 we make some introductory description of the transport-diffusion equation and the limitations of back-trajectories, followed by the basis for adjoint modeling in Section 3. Section 4 covers a formalism for a discrete numerical model needed for the description of influence functions in Section 5. Some numerical aspects are discussed in Section 6, and the adjoint technique is applied to a few events presented in Section 7. The paper in finalized by a summary in Section 8.

2 Transport equation

The fate of a tracer in the atmosphere is described by the continuity equation describing processes in the atmosphere that governs the transport, deposition and transformation. The advection-diffusion equation is a sub-space of the continuity equation omitting processes like chemistry transformation and aerosol dynamics,

$$\frac{\partial \rho\mu}{\partial t} + \nabla \mathbf{v}\rho\mu - \nabla \rho K \nabla \mu + \rho\lambda\mu = q \tag{1}$$

where μ is the mixing ratio of the tracer, ρ air density, $\mathbf{v}$ the mean 3D wind field, K the turbulent diffusion tensor, λ coefficient for wet scavenging and/or radioactive decay, and q the forcing source term . The lower boundary condition of the diffusion term is dry deposition,

$$K_{zz}\frac{\partial \mu}{\partial z}\bigg|_{z=0} = v_d\mu \tag{2}$$

where v_d is the dry deposition velocity.

The basis for trajectories means a further simplification by omitting all terms except the advection,

$$\frac{\partial \rho\mu}{\partial t} + \nabla \mathbf{v}\rho\mu = 0 \tag{3}$$

or combined with the continuity equation for the air itself ($\mu \equiv 1$)

$$\frac{\partial \mu}{\partial t} + \mathbf{v}\nabla\mu = 0 \tag{4}$$

$$\frac{D\mu}{Dt} = 0 \tag{5}$$

where the latter is the total derivative in a Lagrangian framework simply telling us that the mixing ratio is unchanged following an air parcel not exposed to other processes than the transport by the mean wind field.

Apparently the trajectory models oversimplifies the transport processes and are therefore less useful for long time-integrations. Moreover, trajectories are just following one air parcel at the time, i.e. describing a short temporal response at the receptor.

Backward trajectories means following the parcel upstream

$$-\frac{D\mu}{Dt} = 0 \tag{6}$$

$$-\frac{\partial \mu}{\partial t} - \mathbf{v}\nabla\mu = 0 \tag{7}$$

then integrating backwards in time taken the wind field in the reverse direction. In the following section we will show that this is the adjoint of the advection equation (3).

3 Adjoint transport equation

The concept of adjoint operators in this context arises from the Lagrangian duality relation (Marchuk, 1994)

$$< \mu^*, L\mu > = < L^*\mu^*, \mu > \tag{8}$$

where L^* is the adjoint operator of L, μ^* the adjoint control variable, and $<,>$ is an appropriate norm.

Adopting a real valued Euclidean norm

$$< y, x > \quad = \quad y^T x$$

the adjoint equals the transpose

$$< \mu^*, L\mu > \quad = \quad \mu^{*T} L\mu = (L^T \mu^*)^T \mu = < L^T \mu^*, \mu > \tag{9}$$

which is a suitable approach for discrete numerical models and is therefore adopted for the MATCH model. However, some general insight may be gained by investigating a norm in a more general functional space defined over a domain Ω and a time interval T,

$$< g, h > \quad = \quad \int_0^T dt \int_\Omega g h d\Omega$$

and the adjoint in this functional space is defined by,

$$\int_0^T dt \int_\Omega \mu^* f(\mu) d\Omega \quad = \quad \int_0^T dt \int_\Omega \mu f^*(\mu^*) d\Omega \tag{10}$$

As an example we may look into the advection equation (3)

$$\begin{aligned}
\int_0^T dt \int_\Omega \mu^* \left(\frac{\partial \rho\mu}{\partial t} + \nabla \mathbf{v} \rho\mu \right) d\Omega \quad &= \\
\int_0^T dt \int_\Omega \rho\mu \left(-\frac{\partial \mu^*}{\partial t} - \mathbf{v} \nabla \mu^* \right) d\Omega \quad &+ \\
\int_\Omega (\rho\mu\mu^*)_T - (\rho\mu\mu^*)_0 \, d\Omega \quad &+ \\
\int_0^T dt \oint_{\partial\Omega} \mathbf{v} \rho\mu\mu^* \, d\partial\Omega &
\end{aligned}$$

which is derived by partial integration and where $\partial\Omega$ is the boundary of Ω. By applying the constrains $\mu_0 = \mu^*{}_T \equiv 0$, and $\mu^* \equiv 0$ at the boundary $\partial\Omega$, the two latter terms disappear and thus

$$-\frac{\partial \mu^*}{\partial t} - \mathbf{v} \nabla \mu^* \tag{11}$$

is the adjoint to the advection equation (3), and identical with the equation for back-trajectories (7). Back-trajectories are thus the most simplified form of adjoint equations.

For the complete transport and diffusion equation (1) we arrive at,

$$\begin{aligned}
\int_0^T dt \int_\Omega \mu^* \left(\frac{\partial \rho\mu}{\partial t} + \nabla \mathbf{v} \rho\mu - \nabla \rho K \nabla \mu + \rho\lambda\mu \right) d\Omega \quad &= \\
\int_0^T dt \int_\Omega \rho\mu \left(-\frac{\partial \mu^*}{\partial t} - \mathbf{v} \nabla \mu^* - \frac{1}{\rho} \nabla \rho K \nabla \mu^* + \lambda\mu^* \right) d\Omega \quad &+ \\
\int_\Omega (\rho\mu\mu^*)_T - (\rho\mu\mu^*)_0 \, d\Omega \quad &+ \qquad (12) \\
\int_0^T dt \oint_{\partial\Omega_{z\neq 0}} \mathbf{v} \rho\mu\mu^* + \mu\rho K \nabla \mu^* - \mu^* \rho K \nabla \mu \, d\partial\Omega \quad &+ \qquad (13) \\
\int_0^T dt \oint_{\partial\Omega_{z=0}} \mu \rho v_d \mu^* - \mu^* \rho v_d \mu \, d\partial\Omega & \qquad (14)
\end{aligned}$$

with the similar constraints as above, i.e. $\mu_0 = \mu^*{}_T \equiv 0$ and $\mu^* \equiv 0$ at the boundary $\partial\Omega_{z\neq 0}$ (excluding surface boundary), and with the additional constraint $K \equiv 0$ at the boundary $\partial\Omega_{z\neq 0}$ the terms (12) and (13) disappear, while the term (14) incorporates the lower boundary condition (2) at the surface $\partial\Omega_{z=0}$. Hence, the adjoint to the transport-diffusion equations yields,

$$-\rho\frac{\partial\mu^*}{\partial t} - \rho\mathbf{v}\nabla\mu^* - \nabla\rho K\nabla\mu^* + \rho\lambda\mu^* \tag{15}$$

with the lower boundary condition of the diffusion term,

$$K_{zz}\frac{\partial\mu^*}{\partial z}\bigg|_{z=0} = v_d\mu^*. \tag{16}$$

Note that the diffusion and deposition terms are so called self adjoint, i.e. identical in forward and adjoint mode.

4 Discrete numerical model

The MATCH model like other 3D transport models solves the transport-diffusion equation (1) by implementation of different numerical methods on a discrete mesh. Considering all the terms in (1) as linear processes the presentation may be simplified by describing the numerical process in a rather condensed form,

$$\begin{aligned}\mu_0 &= \mu_b\\ \mu_{t+1} &= M_t\mu_t + q\end{aligned}$$

where μ_b is the initial state, and M_t represents all the linear processes treated, μ_t the model state vector on the grid-mesh, t is the time-level, and q the sources term at this stage assumed constant over time. It is convenient to change the model space into a combination of the model state and the source term,

$$z_t = \begin{pmatrix}\mu_t\\ q\end{pmatrix} \tag{17}$$

and the evolution of z_t is thus described by,

$$\begin{aligned}z_{t+1} &= \begin{pmatrix}M_t & I\\ 0 & I\end{pmatrix} z_t\\ &= \mathcal{F}_t z_t.\end{aligned}$$

Generalization to a time-dependent source term is straight forward,

$$\begin{aligned}\mu_0 &= \mu_b\\ \mu_{t+1} &= M_t\mu_t + Q_t q\end{aligned}$$

where Q_t is some time-dependent modulation of the source intensity and location, hence

$$z_{t+1} = \begin{pmatrix}M_t & Q_t\\ 0 & I\end{pmatrix} z_t \tag{18}$$

$$= \mathcal{M}_t z_t. \tag{19}$$

Due to the assumed linearity of the numerical process there is a linear relation between any time level and the initial state,

$$z_t = \mathcal{M}_{t-1}\mathcal{M}_{t-2}\ldots\mathcal{M}_0 z_0 \tag{20}$$

$$z_t = L_0^{t-1} z_0 \tag{21}$$

where L_0^{t-1} then comprises the series of matrix operations $\mathcal{M}_{t-1}\mathcal{M}_{t-2}\ldots\mathcal{M}_0$. It is notable that the matrix $\mathcal{M}$ is never materialized explicitly as the linear processes it comprises could, by the nature of linear processes, be treated separately even on the individual grid-cell level.

5 Influence function

The concept of influence functions may be understood as the area of influence from possible source areas to a given receptor. This is a function of the response time at the receptor and the development of the atmospheric state prior to the response. We should first explore the response from a single observation, and in the next sections evaluate two different approaches to include a set of observations. Let us assume a single observation, $y_{t,i}$, at the time-point t and site i. The model estimate at this point may then be written,

$$\tilde{y}_{t,i} = H_i \mu_t \tag{22}$$

where H_i is a linear observation operator converting the model state to the observed quantities and to the site i. In the most simplest fashion H_i only represents a linear interpolation from the model mesh to the observation point, but could be of more complex nature. Following the notation of z_t in the previous section we may write,

$$\tilde{y}_{t,i} = \begin{pmatrix} H_i & 0 \end{pmatrix} z_t \tag{23}$$

$$= \begin{pmatrix} H_i & 0 \end{pmatrix} L_0^{t-1} z_0 \tag{24}$$

where the latter relation utilizes the linear relation to the initial state ( ). Moreover, we may express this operation by an Euclidean norm and utilize the Lagrangian duality in ( ),

$$\tilde{y}_{t,i} = < \begin{pmatrix} H_i & 0 \end{pmatrix}^T, L_0^{t-1} z_0 > \tag{25}$$

$$= < {L_0^{t-1}}^T \begin{pmatrix} H_i & 0 \end{pmatrix}^T, z_0 > \tag{26}$$

where we can identify that ${L_0^{t-1}}^T$ equals $\mathcal{M}_0^T\mathcal{M}_1^T\ldots\mathcal{M}_{t-1}^T$. We therefore arrive at two different ways to derive the model estimates at the observations points, a) forward integration from time 0 to t and interpolating to the observation site by the observation operator ( ), or b) integrating an adjoint operator $\mathcal{M}_t^T$ backward in time (from t to 0) feed by the observation operator,

$$z_t^* = \begin{pmatrix} H_i^T \\ 0 \end{pmatrix} \tag{27}$$

$$z_{t-1}^* = \mathcal{M}_{t-1}^T z_t^* \tag{28}$$

and thus,

$$\tilde{y}_{t,i} = < z_0^*, z_0 > \tag{29}$$

The impact from deposition processes become visible in Eqn. ( ). Deposition processes are as described above self-adjoint which means that the signal is attenuated when exposed to deposition. This means that the initial state z_0 has to be increased in order to get back to some expected observed value. This is in accordance with that the observation only account for the fraction of the emission that has not been deposited under its way from the source to receptor.

The adjoint control variable z_t^* could be decomposed into the adjoint model state vector and the adjoint emission term, respectively,

$$z_{t-1}^* = \begin{pmatrix} \mu_{t-1}^* \\ q_{t-1}^* \end{pmatrix} \tag{30}$$

$$= \begin{pmatrix} M_{t-1}^T & 0 \\ Q_{t-1}^T & I \end{pmatrix} \begin{pmatrix} \mu_t^* \\ q_t^* \end{pmatrix} \tag{31}$$

where we have taken the transpose of $\mathcal{M}$ in Eqn. ( ), hence

$$\mu_t^* = H_i^T \tag{32}$$

$$\mu_{t-1}^* = M_{t-1}^T \mu_t^* \tag{33}$$

$$q_{t-1}^* = Q_{t-1}^T \mu_t^* + q_t^*. \tag{34}$$

The adjoint control variables should be interpreted in the following way, μ_0^* is the influence function for the initial model state vector, and q_0^* is the influence function reflecting possible emission patterns.

The above implies an inherent assumption that the measurement is instantaneous, as described in ( ), or at least represent the time-resolution of the discrete numerical model (normally a few minutes). However, observations are more likely sampled over several hours or even days. A model estimate would then rather look like,

$$\tilde{y}_t = \frac{1}{N+1} \sum_{\tau=t-N}^{t} H_i \mu_\tau$$

The implication in terms of adjoint backward integration is that the observation operator is repeatedly feed into the adjoint control variables, over the number of time-levels that covers the observation sampling period, scaled by the inverse of the number of model time-steps involved,

$$\begin{aligned} \mu_t^* &= \tfrac{1}{N+1} H_i^T \\ \mu_{t-1}^* &= M_{t-1}^T \mu_t^* + \tfrac{1}{N+1} H_i^T \\ \cdots &\quad \cdots \\ \mu_{t-N}^* &= M_{t-N}^T \mu_{t-N+1}^* + \tfrac{1}{N+1} H_i^T \\ \mu_{t-N-1}^* &= M_{t-N-1}^T \mu_{t-N}^*. \end{aligned} \tag{35}$$

In this fashion the response time is taken into account which is not feasible to achieve in a trajectory model.

5.1 Unit response influence function

In the previous section we presented the meaning of an influence function in terms of one single receptor. Expanding into a set of observations from different sites (that may change over time as well), calls for a measure of the misfit of the model related to the observed values. In this section we will explore a misfit of the first moment, i.e. the mean error, arriving at an influence function with unit response at the receptors. In the next section we will look into the implication of a squared error misfit.

Having access to a set of observations, $y_t = (y_1, y_2, \ldots, y_N)^T$ at a time-level t, the mean error could be represented with a penalty function proportional to the mean deviation between model and measurements,

$$J = \sum_i H_i \mu_t - y_{t,i} = \tag{36}$$

with the same notations as above. We may convert this expression into vector form by introducing a help vector $\hat{I} = (1, 1, \ldots, 1)^T$ defined such that $\hat{I}^T\hat{I} = N$, and a general observation operator H that transform the model state into model estimates at all the observation sites,

$$J = < \hat{I}, H\mu_t - y_t > \quad (37)$$

$$= < \hat{I}, (H \quad 0)\, L_0^{t-1} z_0 - y_t > . \quad (38)$$

Note that $H\mu_t$ has the same dimension as the observation vector y_t. As we will see below, $\hat{I}$ represents a unit response at the observation sites. In the latter expression we have utilised the relation (24) in the previous section. The penalty function in (36) could easily be extended to observations at different observation hours, then incorporating a time-series of measurements.

A perturbation of the penalty function J with respect to the initial state z_0 reads,

$$\delta J = < \nabla J, \delta z_0 > \quad (39)$$

were we could identify that the gradient ∇J is given by,

$$\nabla J = {L_0^{t-1}}^T \begin{pmatrix} H^T\hat{I} \\ 0 \end{pmatrix} \quad (40)$$

$$= \mathcal{M}_0^T \mathcal{M}_1^T \ldots \mathcal{M}_{t-1}^T \begin{pmatrix} H^T\hat{I} \\ 0 \end{pmatrix} \quad (41)$$

which could be evaluated by integrating an adjoint control variable in the following way,

$$z_t^* = \begin{pmatrix} H^T\hat{I} \\ 0 \end{pmatrix} \quad (42)$$

$$z_{t-1}^* = \mathcal{M}_{t-1}^T z_t^* \quad (43)$$

with $\hat{I}$ as the response at the receptors, and thus,

$$\nabla J = z_0^* \quad (44)$$

$$\delta J = < z_0^*, \delta z_0 > . \quad (45)$$

Note the similarity between Eqn. (29) and (45). The the initial state and the emission term, z_0, is given by,

$$z_0 = z_b + \alpha \nabla J \quad (46)$$

where z_b is some initial quess, and α is a coefficient selected in a way that the penalty function (38) is at minimum. For z_b being zero α would represent the emission strength needed to explain the mean value of the observations.

In similar fashion as in the previous section the adjoint control variable z_0^* could be decomposed into the gradient with respect to the initial state and the source function, respectively. Long sampling periods of observed quantities are incorporated in a similar way as described in the previous section, by repeated insertion of the forcing term.

5.2 Weighted influence function

We have shown that an influence function based on a mean error penalty function leeds to an unit resonse at the receptors that does then not reflect the individual magnitudes

of the observations. In the following we will borough the basis for data assimilation at the end arriving at an influence function that is weighted by the observed quantities.

In variational Bayesian data assimilation an initial guess is modified by minimizing a penalty function of the following kind,

$$\begin{aligned} J(z) &= \tfrac{1}{2}(z - z_b)^T B^{-1}(z - z_b) + \tfrac{1}{2}(y - \tilde{y}(z))^T O^{-1}(y - \tilde{y}(z)) \\ &= J_b + J_o \end{aligned}$$

where z_b is the initial guess, B and O are covariance matrices representing background and observation errors, respectively, and $\tilde{y}$ is the model estimate at observation points similar to Eqn. (22) (see e.g. Lorenc, 1986, Courtier et *al.*, 1993).

In this context we will only consider the observation term (J_o) and further simplify by setting the observation errors to unity. By introducing our model state z_t from Eqn. (17) we arrive at,

$$J_o(z_t) = \tfrac{1}{2}(y_t - \tilde{y}_t(z_t))^T (y_t - \tilde{y}_t(z_t))$$

and using the results from Talagrand and Courtier (1986) demonstrating that the gradient of J_o with respect to z_0 is given by,

$$-\nabla J_o(z_0) = \mathcal{M}_0^T \mathcal{M}_1^T \ldots \mathcal{M}_{t-1}^T \begin{pmatrix} H^T \\ 0 \end{pmatrix} (y_t - \tilde{y}_t(z_0))$$

where we have used the linear relation between z_t and z_0 in (20). In data assimilation the gradient is used in order to iteratively find the optimal selection of μ_0 and q that fits to the observed data (Talagrand and Courtier, 1987, Derber, 1989, Robertson and Persson, 1993). The scope of this paper, however, is just to get a first glance at the possible source regions. Therefore we omit the the forward contribution, $\tilde{y}_t$, implying a first forward estimate being an imaginary run with no initial state and no emissions.

The gradient is then the influence function weighted by the observations. This gradient may, in a similar fashion as for Eqns. (27) - (34), be found by integrating adjoint control variables by the following scheme,

$$\mu_t^* = H^T y_t \quad (47)$$

$$\mu_{t-1}^* = M_{t-1}^T \mu_t^* \quad (48)$$

$$q_{t-1}^* = Q_{t-1}^T \mu_t^* + q_t^* \quad (49)$$

arriving at

$$-\nabla J_o(z_0) = -\begin{pmatrix} \nabla J_o(\mu_0) \\ \nabla J_o(q) \end{pmatrix} = \begin{pmatrix} \mu_0^* \\ q_0^* \end{pmatrix}.$$

The difference from the unit response adjoint relation is that the observation vector y_t replaces the unit vector $\hat{I}$ (see e.g. Eqn. 42). Moreover, for inert substances the gradient would directly reflect the emission rate. However, when deposition processes are included the gradient will be attenuated, which make sense in a data assimilation procedure, but in our application the direct interpretation as emission rate is lost.

In a similar fashion as in (35) observed values sampled over a longer time-period is repeatedly feed into the adjoint control variable.

The weighted influence function puts a certain emphasis in pointing out source regions that are able to explain the largest measured values. It is also possible to directly deduce the source intensity from the weighted influence function, under the condition that deposition could be omitted.

6 Numerical aspects

There are some numerical considerations worth mentioning before looking into the examples. Noted in Section 4 various numerical methods are used to solve the advection-diffusion equation (1) on the discrete grid-mesh. As an example we should look into the advection term that is solved in the MATCH model by a donor cell approach (Robertson et *al.*, 1999),

$$\begin{aligned} \mu_{t+1}^{i+1} &= \mu_t^{i+1} + F^+ \\ \mu_{t+1}^{i} &= \mu_t^{i} - (F^+ + F^-) \\ \mu_{t+1}^{i-1} &= \mu_t^{i-1} + F^- \end{aligned} \tag{50}$$

where the indices μ_t refers to the time-level, and μ^i to the grid-cell index. The fluxes (F^+ and F^-) are calculated at the grid-cell μ^i and donated to its neighbors. This is a flux oriented scheme that guarantees mass conservation. For a second order scheme the fluxes are calculated utilizing the three adjacent grid-cells,

$$\begin{aligned} F^+ &= a^+\mu^{i+1} + b^+\mu^i + c^+\mu^{i+1} \\ F^- &= a^-\mu^{i+1} + b^-\mu^i + c^-\mu^{i+1} \end{aligned}$$

where a, b, c are Lagrangian polynomial functions taking the wind field as argument. In higher order schemes more grid-cells are involved in the flux calculations, giving a higher degree of accuracy. Rephrasing (50) in a linear form yields,

$$\begin{pmatrix} \mu^{i+1} \\ \mu^i \\ \mu^{i-1} \end{pmatrix}_{t+1} = \begin{pmatrix} \mu^{i+1} \\ \mu^i \\ \mu^{i-1} \end{pmatrix}_t + \begin{pmatrix} a^+ & b^+ & c^+ \\ -a^+ & -b^+ & -c^+ \\ 0 & 0 & 0 \end{pmatrix} \begin{pmatrix} \mu^{i+1} \\ \mu^i \\ \mu^{i-1} \end{pmatrix}_t + \begin{pmatrix} 0 & 0 & 0 \\ -a^- & -b^- & -c^- \\ a^- & b^- & c^- \end{pmatrix} \begin{pmatrix} \mu^{i+1} \\ \mu^i \\ \mu^{i-1} \end{pmatrix}_t$$

and the adjoint (transpose) of this linear system is given by,

$$\begin{pmatrix} \mu^{i+1} \\ \mu^i \\ \mu^{i-1} \end{pmatrix}_t = \begin{pmatrix} \mu^{i+1} \\ \mu^i \\ \mu^{i-1} \end{pmatrix}_{t+1} + \begin{pmatrix} a^+ & -a^+ & 0 \\ b^+ & -b^+ & 0 \\ c^+ & -c^+ & 0 \end{pmatrix} \begin{pmatrix} \mu^{i+1} \\ \mu^i \\ \mu^{i-1} \end{pmatrix}_{t+1} + \begin{pmatrix} 0 & -a^- & a^- \\ 0 & -b^- & b^- \\ 0 & -c^- & c^- \end{pmatrix} \begin{pmatrix} \mu^{i+1} \\ \mu^i \\ \mu^{i-1} \end{pmatrix}_{t+1}$$

or

$$\begin{aligned} \mu_t^{i+1} &= \mu_{t+1}^{i+1} + a^+(\mu^{i+1} - \mu^i)_{t+1} + a^-(\mu^{i-1} - \mu^i)_{t+1} \\ \mu_t^{i} &= \mu_{t+1}^{i} + b^+(\mu^{i+1} - \mu^i)_{t+1} + b^-(\mu^{i-1} - \mu^i)_{t+1} \\ \mu_t^{i-1} &= \mu_{t+1}^{i-1} + c^+(\mu^{i+1} - \mu^i)_{t+1} + c^-(\mu^{i-1} - \mu^i)_{t+1}. \end{aligned} \tag{51}$$

Note that the forward scheme in flux form (50) are turned into difference form in the adjoint scheme (51), similar to the analytical formulations in Eqns. (3) and (11) that transforms the advection term from flux form to advective form.

From a numerical point of view the difference form in (51) is a numerically unstable scheme, causing oscillations and negative values. In order to minimize this deficiency a low-pass Forester filter (McRae et *al.*, 1982) is applied. Figure 1 illustrates the impact of filtering for a second order adjoint advection scheme, and the importance of filtering is rather evident.

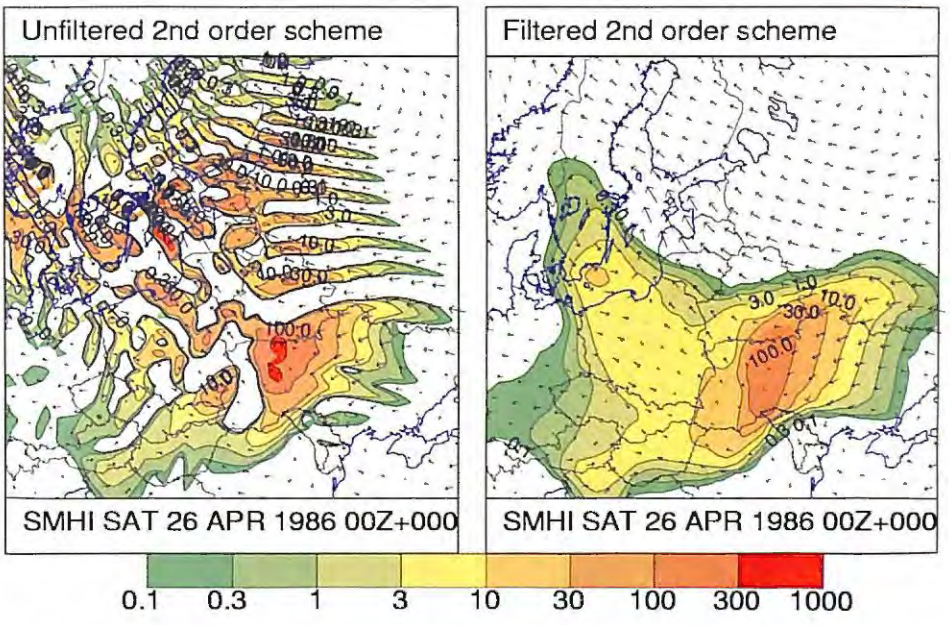

Figure 1: *Adjoint simulation with and without Forester filter for a second order advection scheme.*

The selection of advection scheme is a delicate balance between numerical accuracy and computation speed. In Figure 2 the results from four different adjoint advection schemes are shown. There are not that much gain from higher order schemes, while the fastest (zero order) scheme is all too diffusive. The second order scheme is hereafter used in the examples to follow.

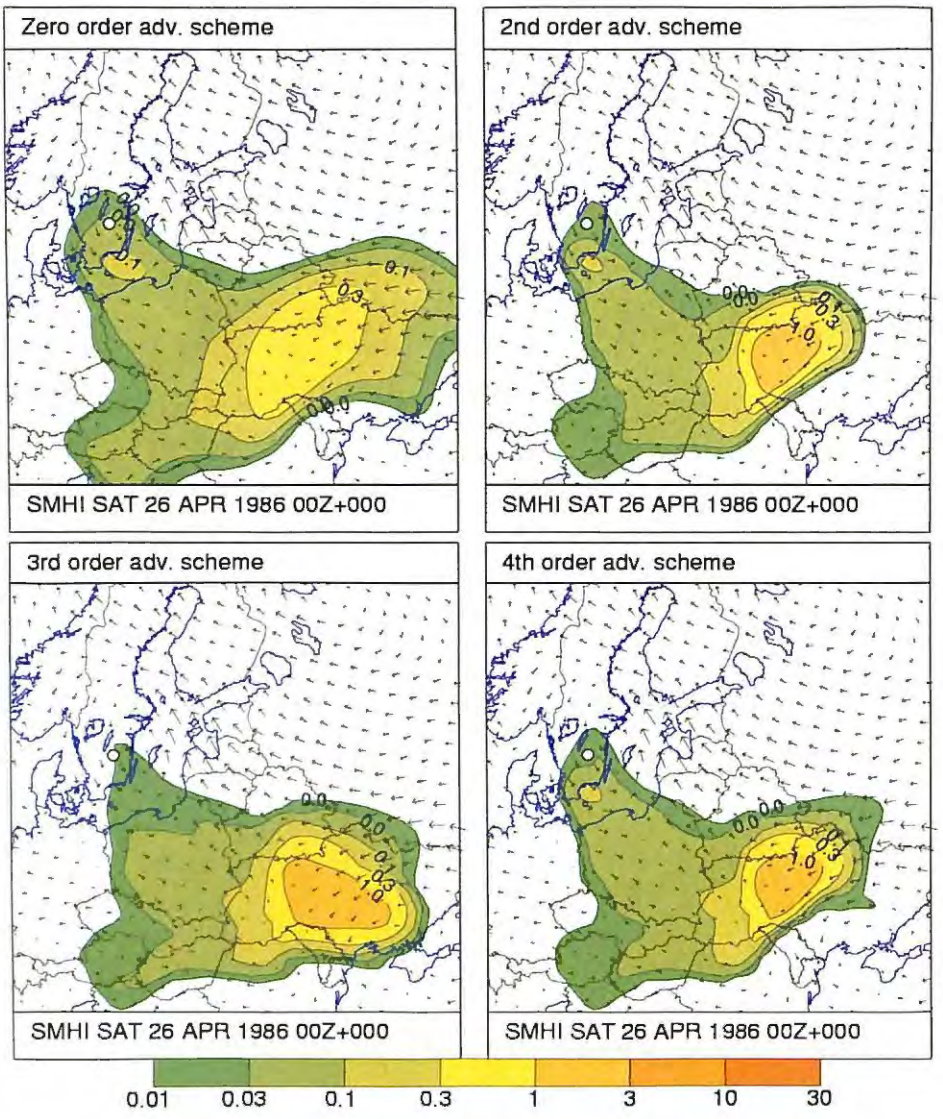

Figure 2: *Demonstration of various adjoint advection schemes, ranging from zero order (upstream) (upper left) to forth order (lower right). The figure shows that a second order scheme appears sufficient, and is thus selected in the examples.*

7 Examples

In the following examples we will demonstrate the potential of extended back-trajectories, and the implications of using either unit response or weighted influence functions. The first example is taken from the Chernobyl accident followed by the ETEX tracer experiment. Next we use the Algeciras accident to investigate the implications of measurements with various sampling periods, and the final example is an event with heavy smoke from Eastern Europe. Finally, a suggestion for an operational setup is discussed.

The deposition processes have been excluded in these examples.

7.1 The Chernobyl accident

The Chernobyl accident took place in the morning 26 April 1986 around 00 UTC. Measurements where taken all over Europe, while we have restricted this demonstration to a selection of mainly Swedish samples. The observations used are from Stockholm, Eksjö, Oskarshamn, Ringhals, Ljungbyhed, Öland and Risø (Persson et al., 1987). Figure 3 shows the readings for a selection of these locations. As seen from the figure there are two occasions where the radioactive cloud passed Scandinavia.

In Figure 4 the first episode is followed backwards and hit an area around the Chernobyl plant at 00 UTC the 26 April 1986. The figure shows the weighted influence function based on all observations from 1 of May and earlier. By using the weighted influence function the individual magnitudes of observed values are taken into account in the adjoint simulation.

Figure 5 shows the time-series of the weighted influence function at the location of Chernobyl and for different heights using all observation from 26 April to 10 May. The influence function reflects the source term and demonstrates that there was a second part of accidental emission that made its way towards Scandinavia.

However, in lack of available observations this type of simulation is not feasible. Having just an indication of elevated radioactivity at these stations the unit response influence function becomes the only means of assessment (see Section 5.1). We have chosen to use observations exceeding 0.1 Bq/m^3 as indications of the timing at the receptors, and thus assigned a unit response for these values. Figure 6 illustrates the time-series for unit response influence function at Chernobyl. It becomes clear that the unit response approach is more for a qualitative indication of impact from a given source point rather than a quantification of the emission rate.

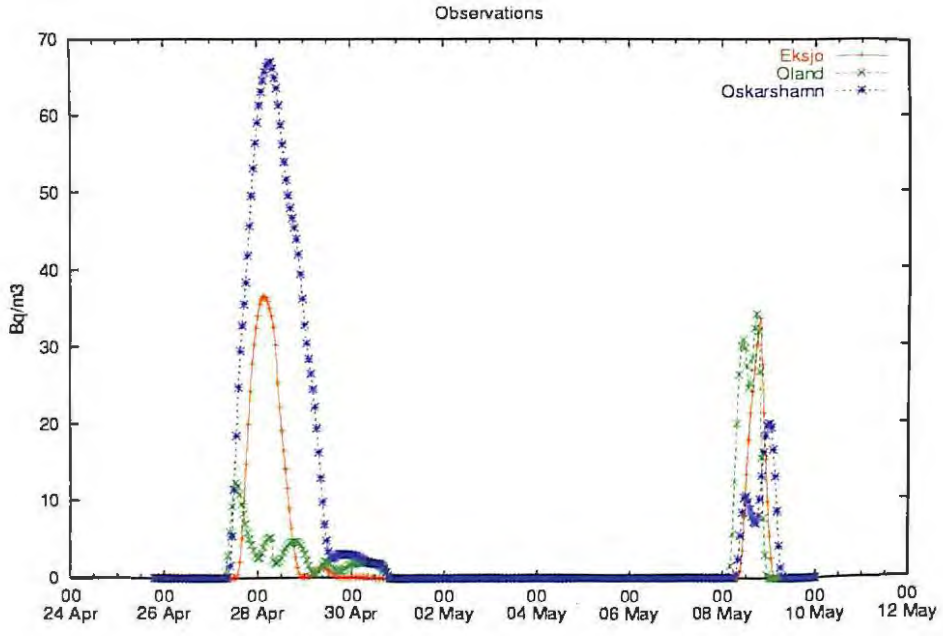

Figure 3: *Measured values of Cs^{137} at Eksjö, Öland and Oskarshamn, respectively, in April and May 1986. Unit in Bq/m^3.*

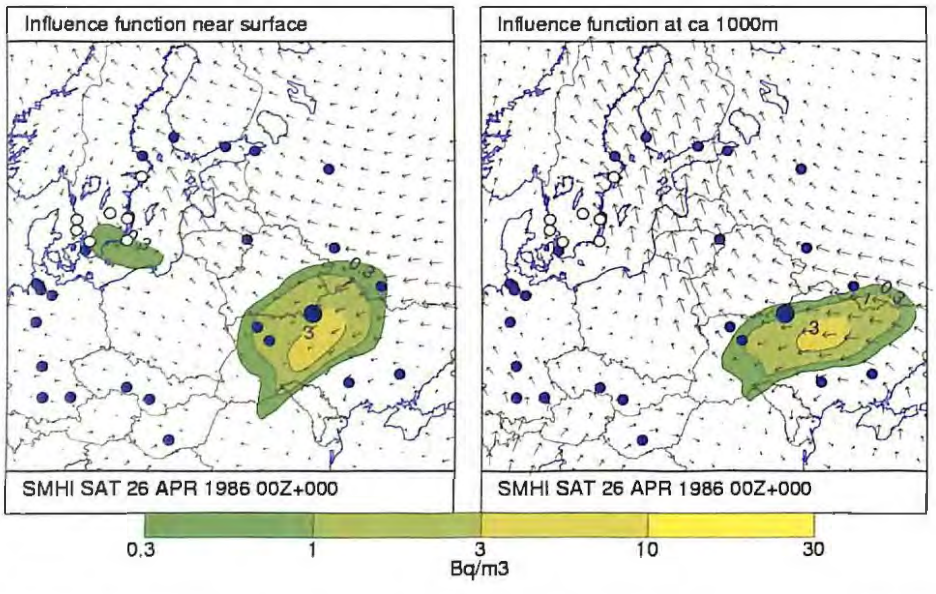

Figure 4: *Weighted influence function for the first occasion when the radioactive cloud from Chernobyl reached Sweden, calculated from 1986-05-01:00 back to 1986-04-26:00, and using all the available observations over this period. Unit in Bq/m^3. The empty circles point out the observation sites, and the filled circles are various nuclear power plants in this area. The large filled circle point out the location of Chernobyl.*

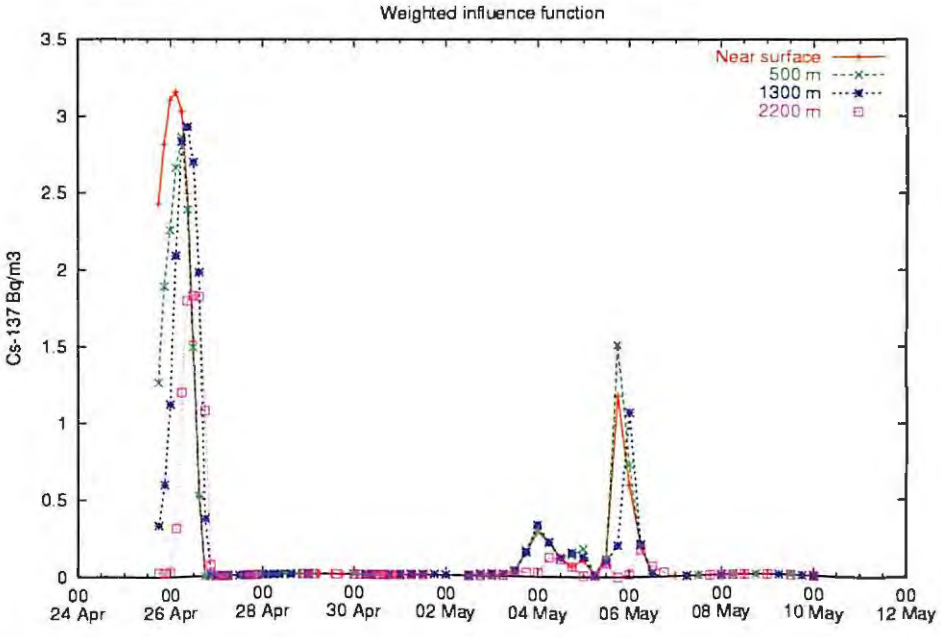

Figure 5: *Time series of the weighted influence function at Chernobyl for different heights. Unit in* Bq/m^3.

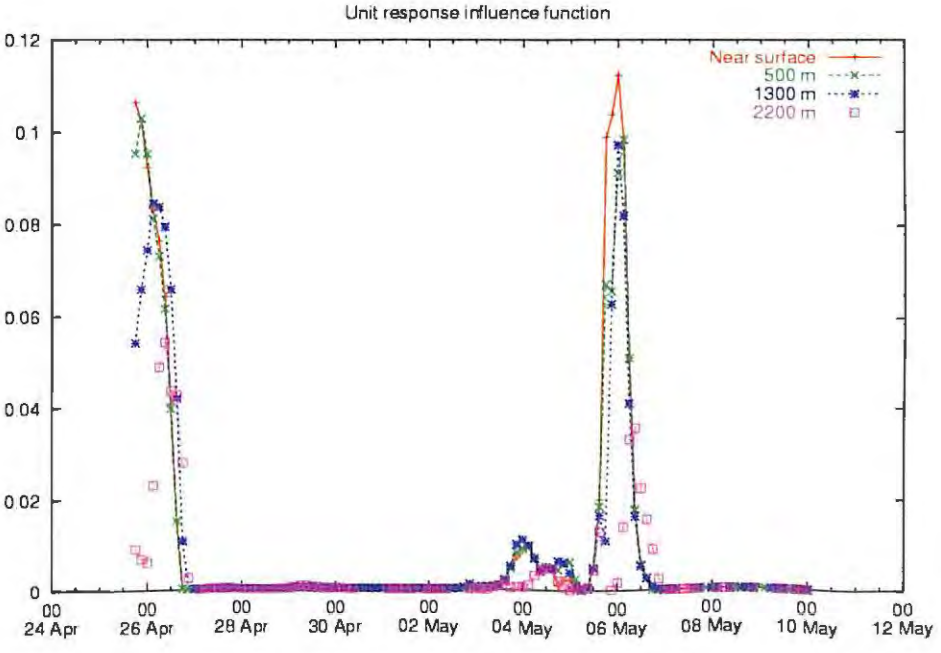

Figure 6: *Time series of the unit response influence function at Chernobyl for different heights. Non-dimensional unit.*

7.2 ETEX experiment

The European Tracer Experiment (ETEX) provides two data sets from controlled point source releases monitored across Europe. The experiments took place in late October (ETEX-I) and early November (ETEX-II), 1994. The former of these two data sets has been used here. In both experiments a perflourocarbon (PFC) was released into the atmosphere in Monterfil, Brittany (France), over a period of 12 hours at a rate of 7.9 g/s, and air samples were taken at 168 stations in 17 European countries up to 90 hours after the start of the release (Nodop *et al.*, 1997). The tracer was sampled in 3-hour intervals and for ETEX-I a total of 3104 measurements passed the quality control. The PFC is an inert gas insensitive to uptake at the surface or wet scavenging, and is thus only affected by advection and diffusion.

Figure 7 shows the adjoint simulation at four different instances. In the lower right panel the influence function is given at the center data of the "true" release period, and displays its maximum at the release point.

In Figure 8 time-series of the influence function is plotted for different heights. The tracer experiment was a near surface release that is reproduced in this adjoint simulation.

The time-series in Figure 9 is a transform into an emission rate of the concentration profiles in Figure 8, which is doable as deposition is not active for an inert tracer, therefor is all emission transferred to the observation points with no losses during transport. This source rate is a factor two less than the true release. This may have several reasons, the observations may not "see" more of the release, the MATCH model may have a bias that affect the emission estimate. This brings forward that any emission estimate is always model dependent, and has to evaluated having this in mind.

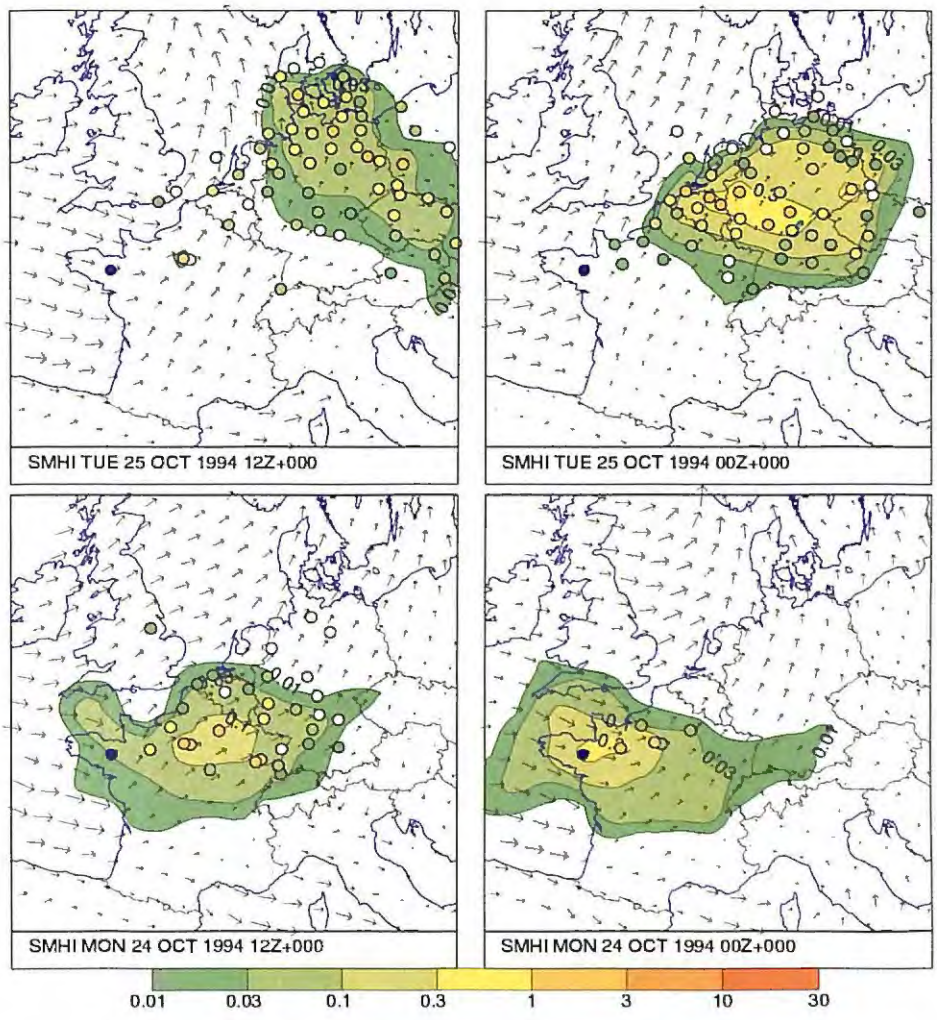

Figure 7: *Weighted influence function at four different dates for the ETEX I case. Note that the integration is made backward. Unit in* ng/m^3

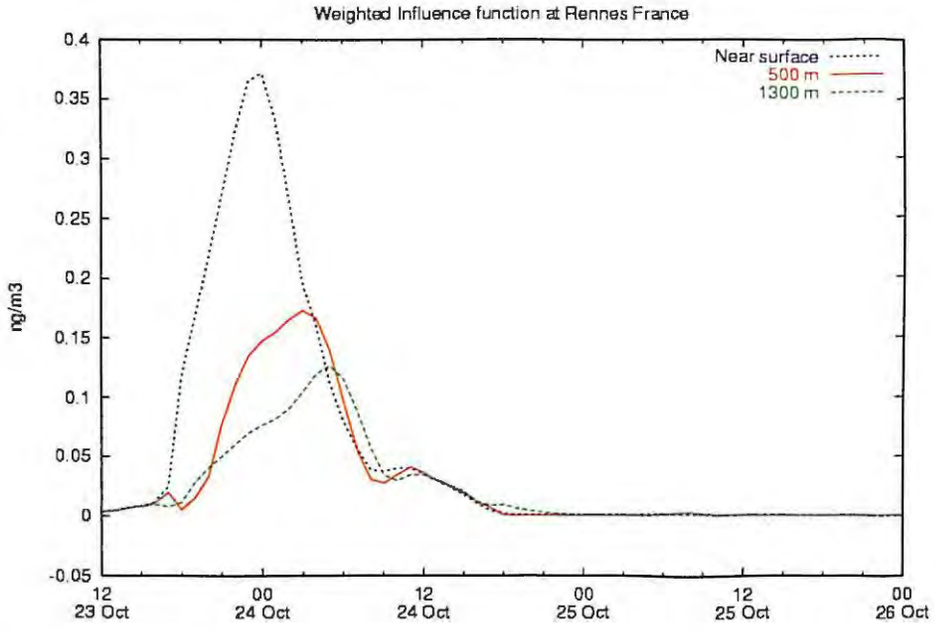

Figure 8: *Time-series of the weighted influence function at the source location of the ETEX experiment, and at different heights. Unit in* ng/m^3.

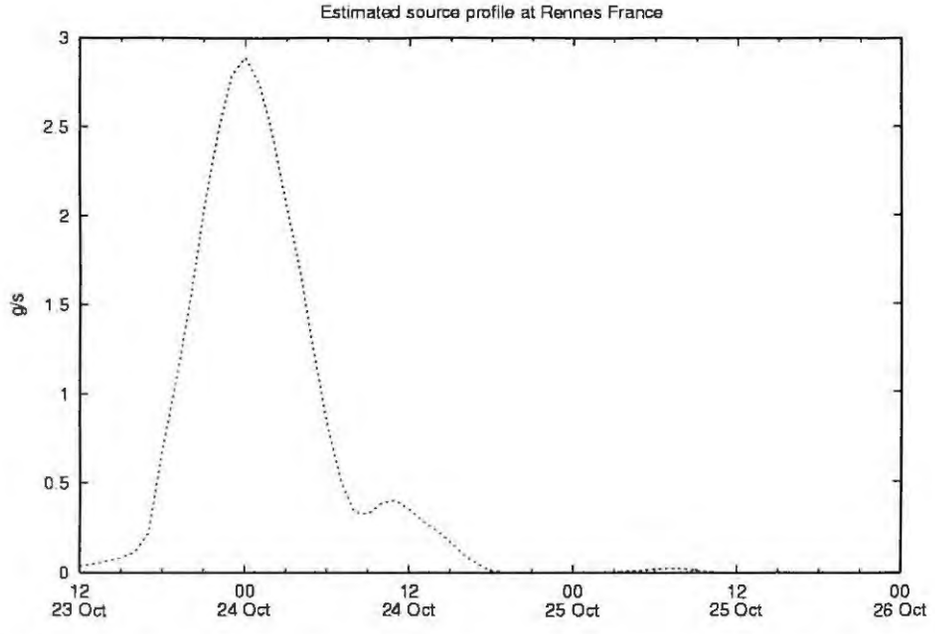

Figure 9: *Estimated source function for the ETEX experiment, where the results in Figure 8 are used. Unit in* g/s.

7.3 Algeciras accident

In the spring-time of 1998 an accidental release of Cs^{137} occurred from the steel mill Acerinox close to Algeciras, Spain. The release was estimated to 8 - 80 Ci over a few hours period in the morning of 30 May (00 - 03 UTC). The health effect was concluded to be well below exposure limits. Vogt et *al.* (1998) compiled a number of filter measurements across Europe and also made the first estimates of the release amount. The measurements comprises a data set with a wide range of sampling times, from 1 day up to 14 days, and cover the period from 2 June to 17 June.

We have split the data into 3 different datasets: 1) all data, 2) measurements sampled for 1 day, and 3) measurements sampled for more than one day, respectively.

In the Figures 10 and 11 the weighted influence function is plotted for 4 different instances, and with the dataset 2 and 3, respectively. The discussion on the forcing from observations sampled over longer periods, in Section 5, is especially valid for this case. An equal fraction of the observed values are reinserted into the adjoint model for 1 up to 14 days in this example.

In Figure 10 it is notable the bifurcation starting at 31 May 00 UTC and leading to a double peak over Spain, one at the Algeciras location and one in central Spain. The dataset 3, representing long term samples, used in Figure 11 result in a less distinct influence function as could be expected.

The time-series plots in Figures 12, 13 and 14 clearly shows that most of the signal comes from the short term measurements. Still the long term observations are able to provide some information, even though not entirely unambiguous. The bifurcation displayed in Figure 10 implies that several source locations are possible, and only the precise timing of the release would discriminate the most probable one from the others. In these latter figures the weighted influence function is transformed into emission estimates (Ci/h) showing peak numbers that are in accordance with the estimated total release of 8 - 80 Ci. However, deposition processes are not accounted for in these simulations which make the emission estimates a bit dubious.

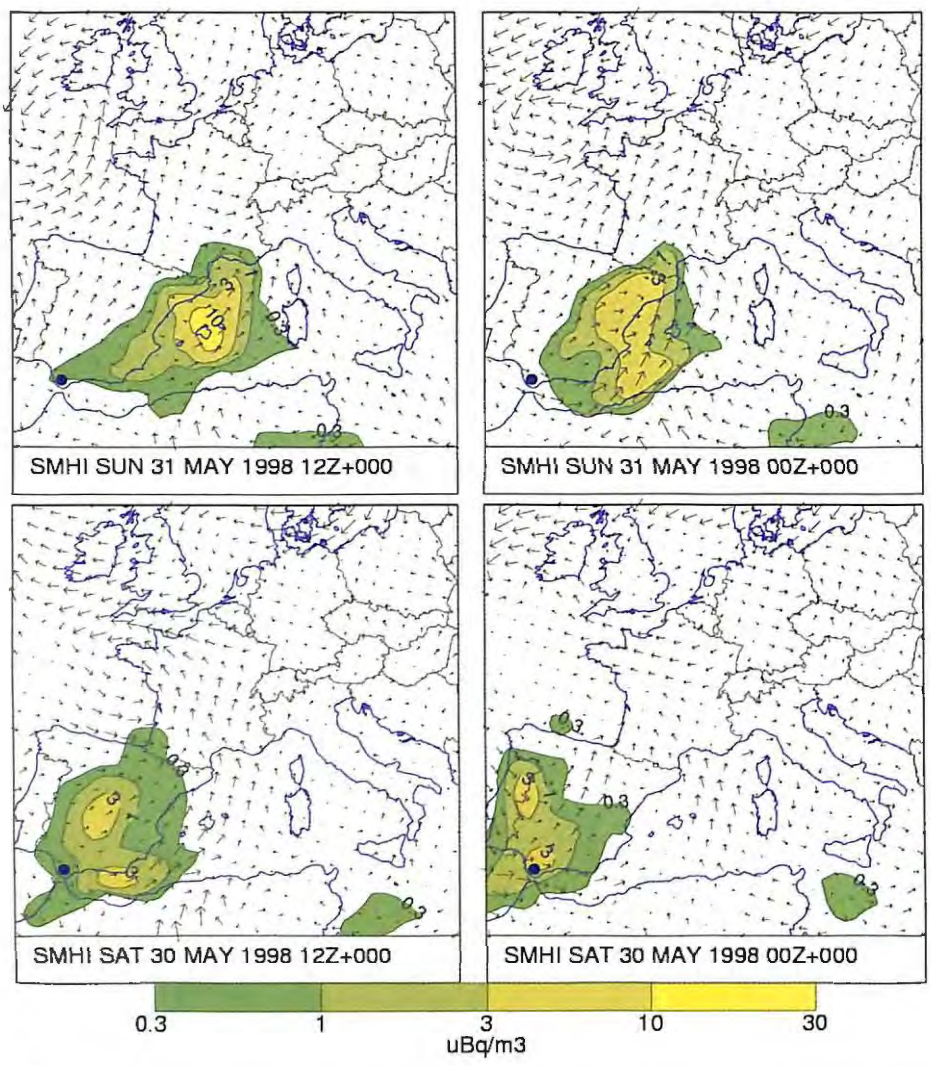

Figure 10: *The weighted influence function at 4 different instances using observations from the Algeciras accident with sampling time of 1 day. The filled circle in southern Spain points out Algeciras.*

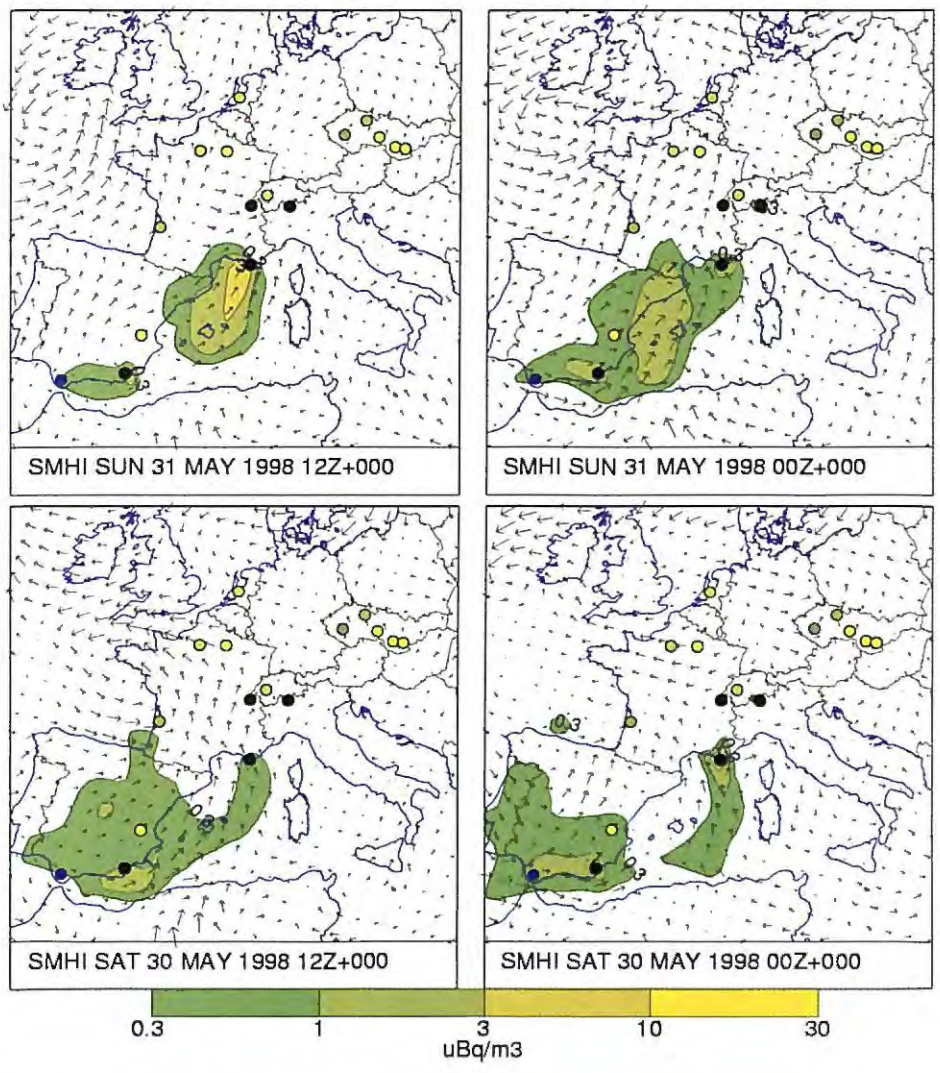

Figure 11: *The weighted influence function at 4 different instances using observations from the Algeciras accident with sampling time more than 1 day. In addition to the location of Algeciras in southern Spain the other circles are the long term measurements available at the different dates. Black filled circles means that the observations values exceeds the color scale.*

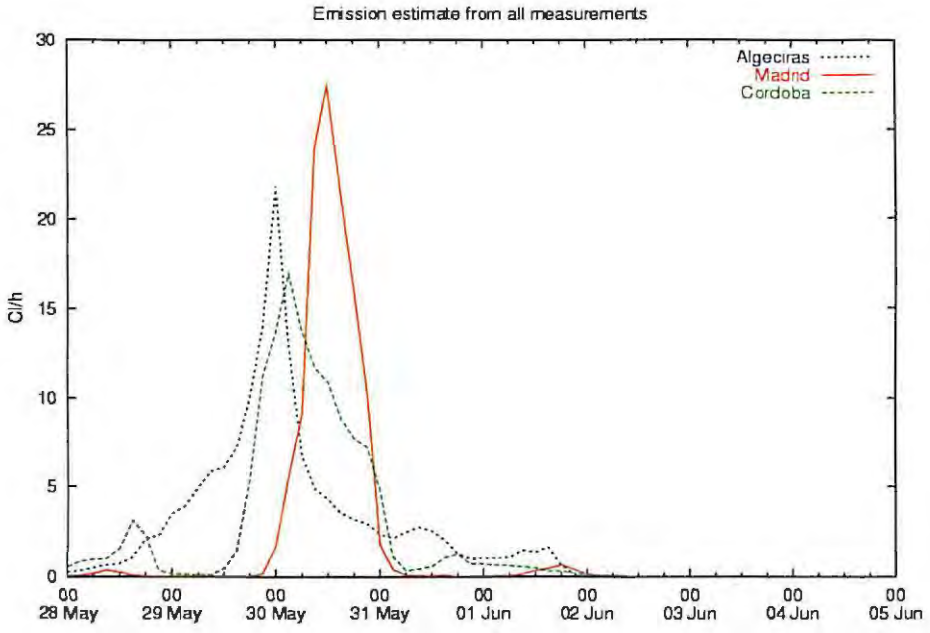

Figure 12: *Time-series of the weighted influence function transformed into an emission estimate (Ci/h) at three different locations including Algeciras where all available observations are used.*

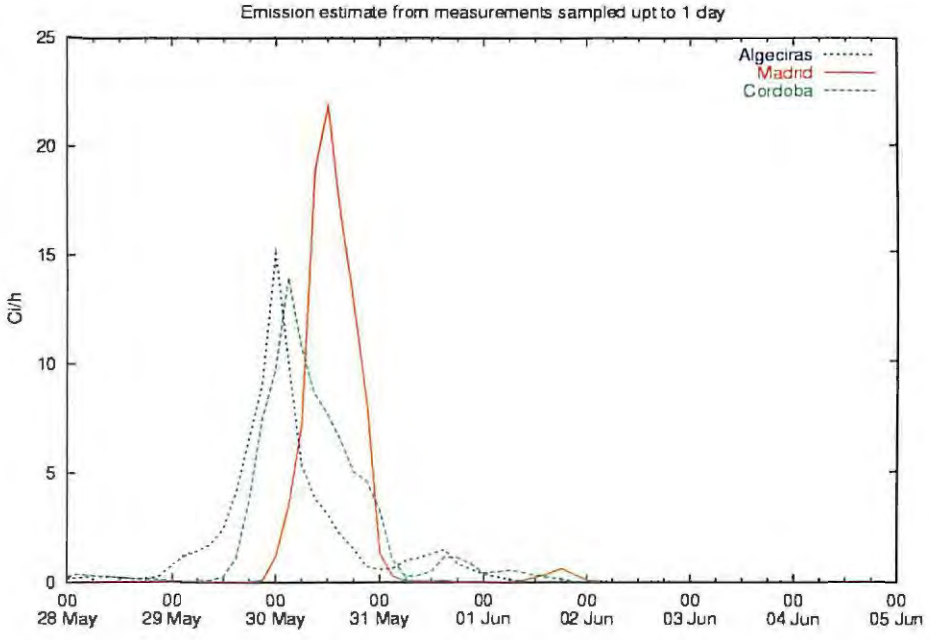

Figure 13: *Time-series of the weighted influence function transformed into an emission estimate (Ci/h) at three different locations including Algeciras where observations sampled up to 1 day are used.*

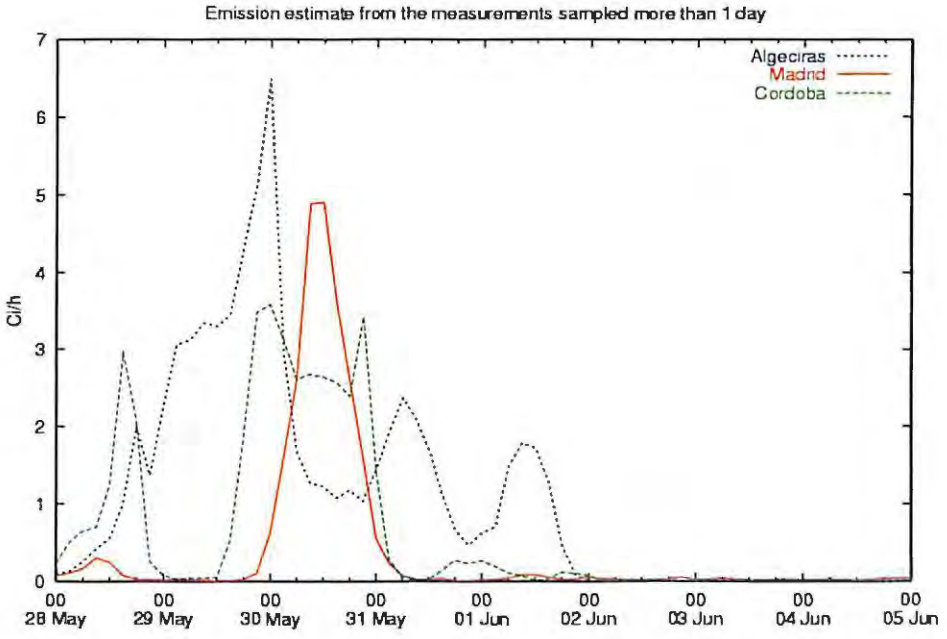

Figure 14: *Time-series of the weighted influence function transformed into an emission estimate (Ci/h) at three different locations including Algeciras where observations sampled over more than 1 day are used.*

7.4 Heavy smoke incident in Scandinavia

In the beginning of September 2002 smoke particles where noticed in southern Sweden. The origin was at first unclear but a lot of observations over a large area indicated long-range transport. At the time assumptions where made that severe forest fires reported from the Moscow area, Russia, could be the reason. We may however conclude that the Moscow fires did not contribute to this smoke to any significant degree.

The smoke was sufficiently dense to affected the visibility observed at synoptic weather stations in southern Sweden. Figure 15 shows some of the visibility readings from 3 to 8 September, 2002. The most profound drop in the visibility occurred 4 - 5 and 7 September, with some recovery during 6 September.

In this experiment we assumed visibility below 5 km to be associated with this smoke event, and we formed a control variable taking the visibility as argument,

$$c(V) = \frac{5 - min(V, 5)}{5} \tag{52}$$

where the visibility, V, is measured in km. Figure 16 shows the visibility records for the two weather stations in Figure 15 converted into this control variable. In total visibility observations from 11 synoptic station in southern Sweden have been used.

Figure 17 shows the adjoint simulation that clearly indicating source regions in central Europe. Integration towards earlier dates does not show any influence from the Moscow area. Information about a number of forest fires in northern Ukraine (Yaroslav Sorokin at Institute of Mathematical Machines and System Problems, Kiev, Ukraine, personal communication) make us more convinced that forest fires in central Europe contributed to the smoke noticed rather than forest fires from the Moscow area.

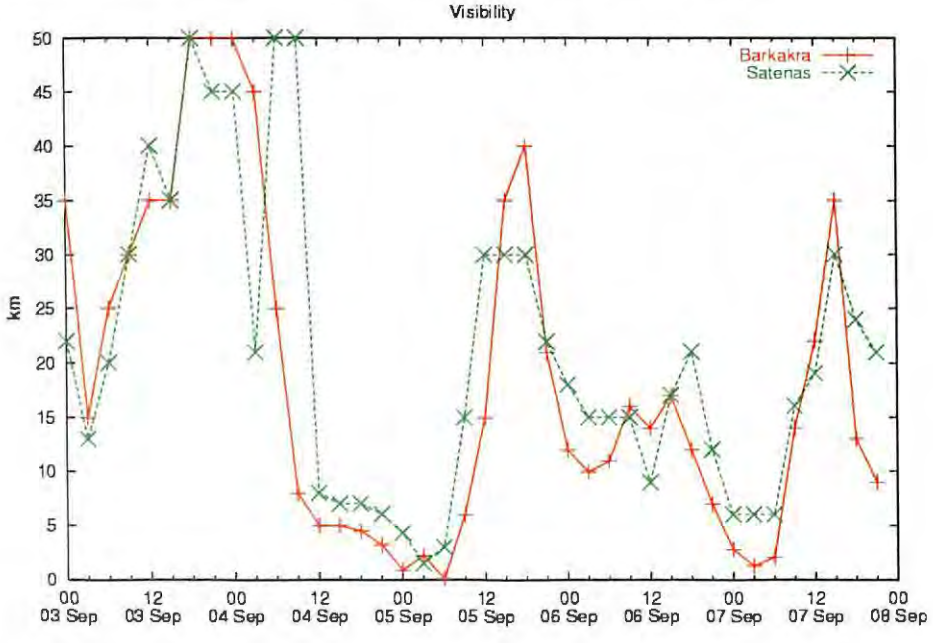

Figure 15: *Time-series of visibilities at two locations in Southern Sweden, Barkåkra and Sätenäs, in early September 2002.*

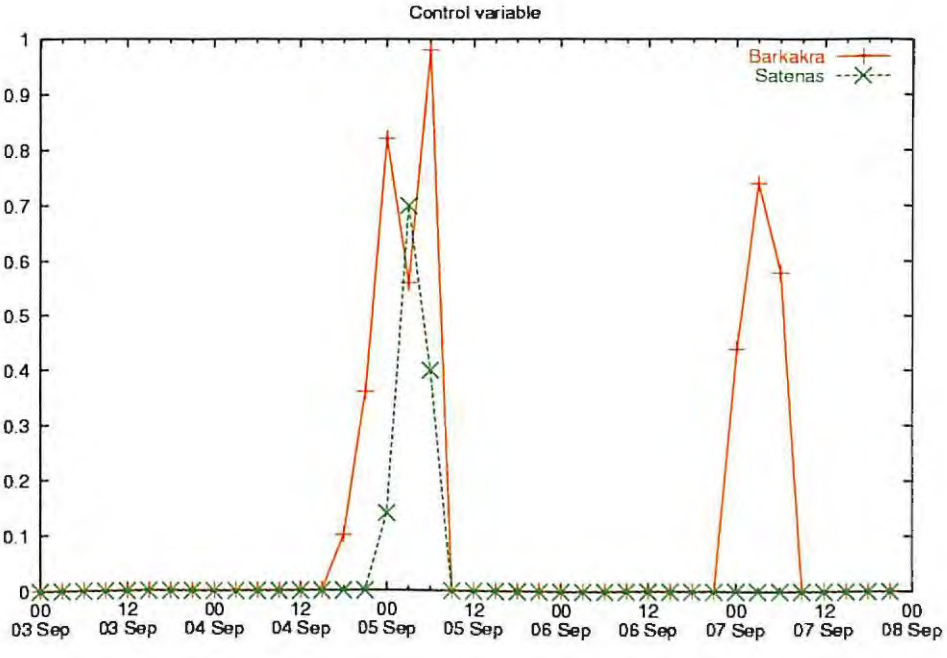

Figure 16: *The time-series in 15 transformed into a control variable used in the adjoint simulations.*

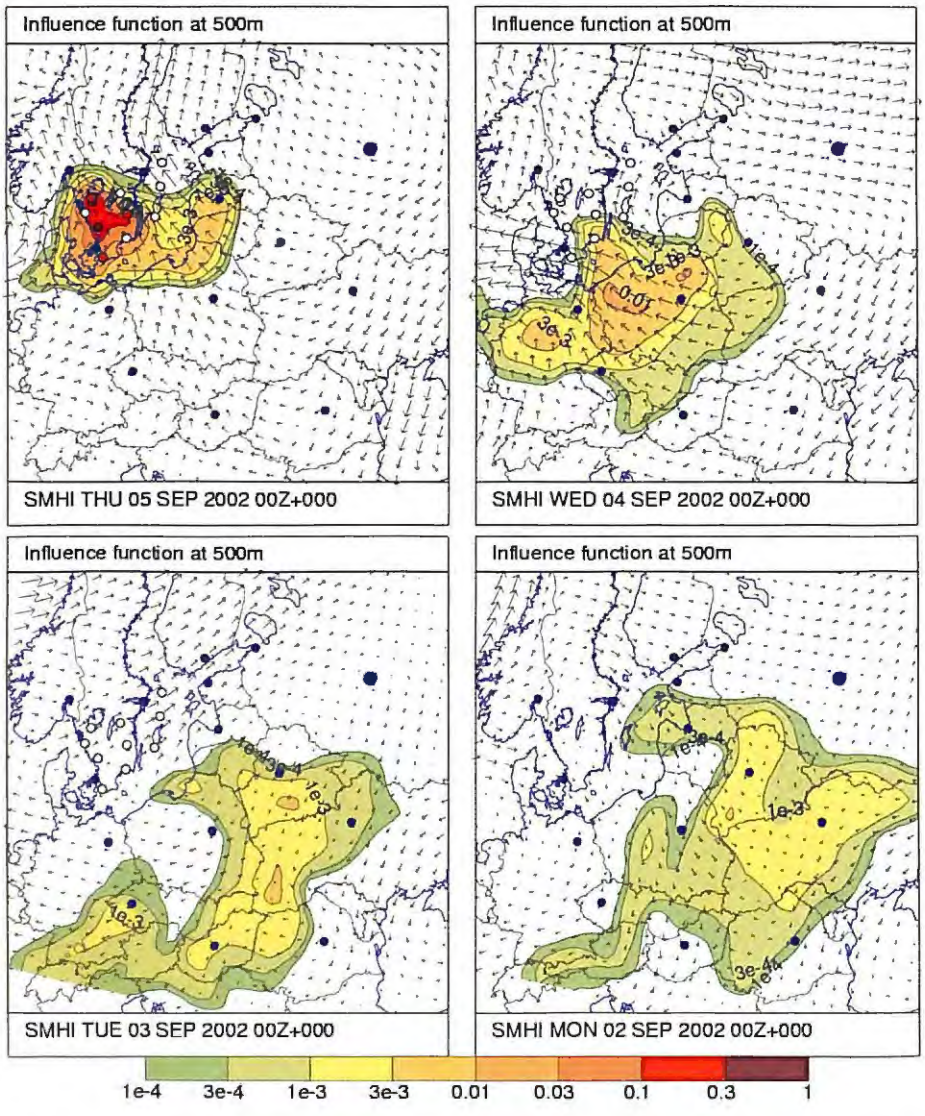

Figure 17: *Backward transport of transformed visibility observations. Some major cities are plotted as blue filled circles. In the text we discuss the importance from Moscow area that is the somewhat larger circle to the north-east.*

7.5 An operational approach

In the previous examples we have demonstrated the use of various observations from some selected events. An operational approach has, however, to be based on routine procedures where measurements are not likely to be available. More over, results should be made accessible before any measurements are taken and provide a quick guidance of possible source origins in case the information will be needed. We are then restricted to the use of the unit response approach.

Figure 18 shows an example of the present operational products now available with the back-trajectories for some selected receptor points. In Figure 19 we have added adjoint modeling combined with traditional back-trajectories for one of the receptors. In this specific example it becomes clear that trajectories have limitations in describing the atmospheric transport, but would anyhow provide some useful information. We have restricted the calculations to only one of the receptors in Figure 18 simply because influence functions from several receptors will be superimposed in the presentation and not possible to be separated from each other.

In the figure the influence function originates from a unit response of a 6 hour period over a depth of 500m at the receptor. Trajectories are calculated with start dates at the end of this period and for a start height of 300m. Figure 20 shows plain trajectory plots for comparison. An optional product would be the mean influence function as shown in Figure 21, but could on the other hand be a bit ambiguous.

In the example given the influence function became rather elongated during the course of integration, in contrast to the next example in Figure 22 where the influence area is more like a moving blob, and as shown in Figure 23 the mean influence function displays a more confined track of possible emission areas.

In a web based product dissemination the standard products as in Figure 18 could be the entry point, where the various receptor points could be made click-able in order to display the adjoint simulations for each receptor.

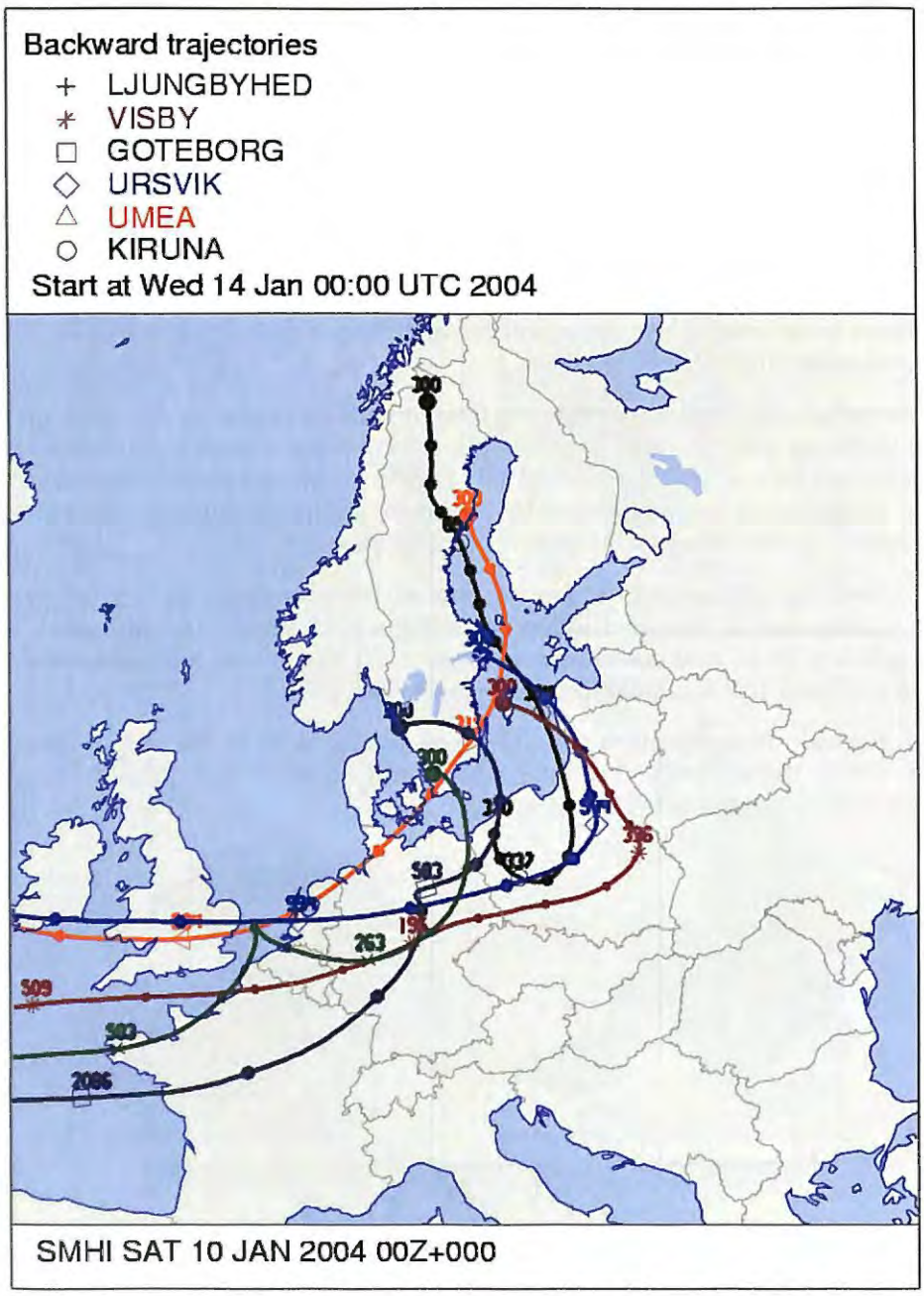

Figure 18: *Example of the present operational product of back-trajectory calculations. The symbol denoting a given receptor appears for every 24 hour along the trajector, and minor filled cricles appear at every 6 hour.*

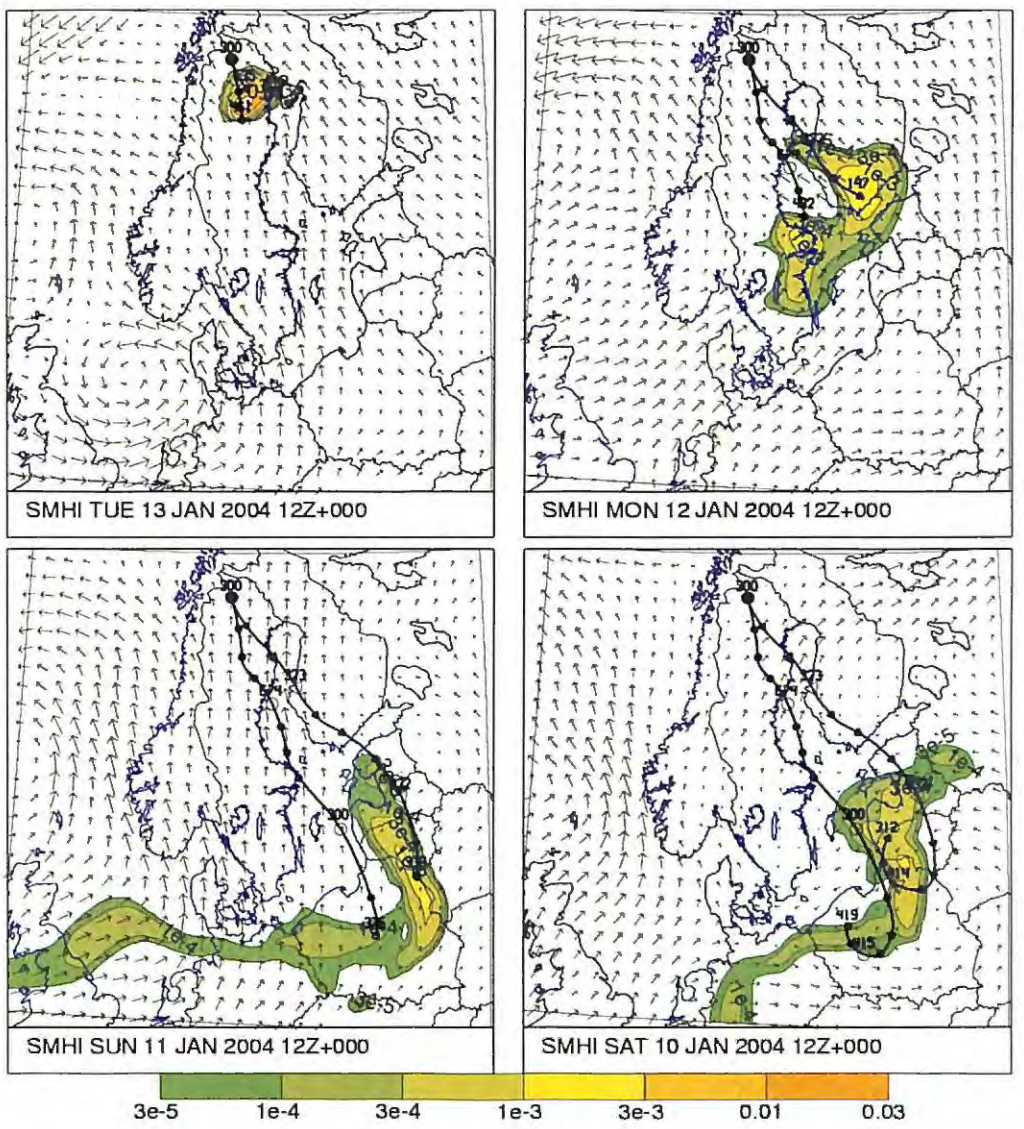

Figure 19: *Unit response influence function for a 6 hour response at Kiruna and trajectories starting in both ends of the response period. The black line with circles starts at 09-14:00 UTC and the blue line with triangles at 09-13:18 UTC. Non dimensional unit.*

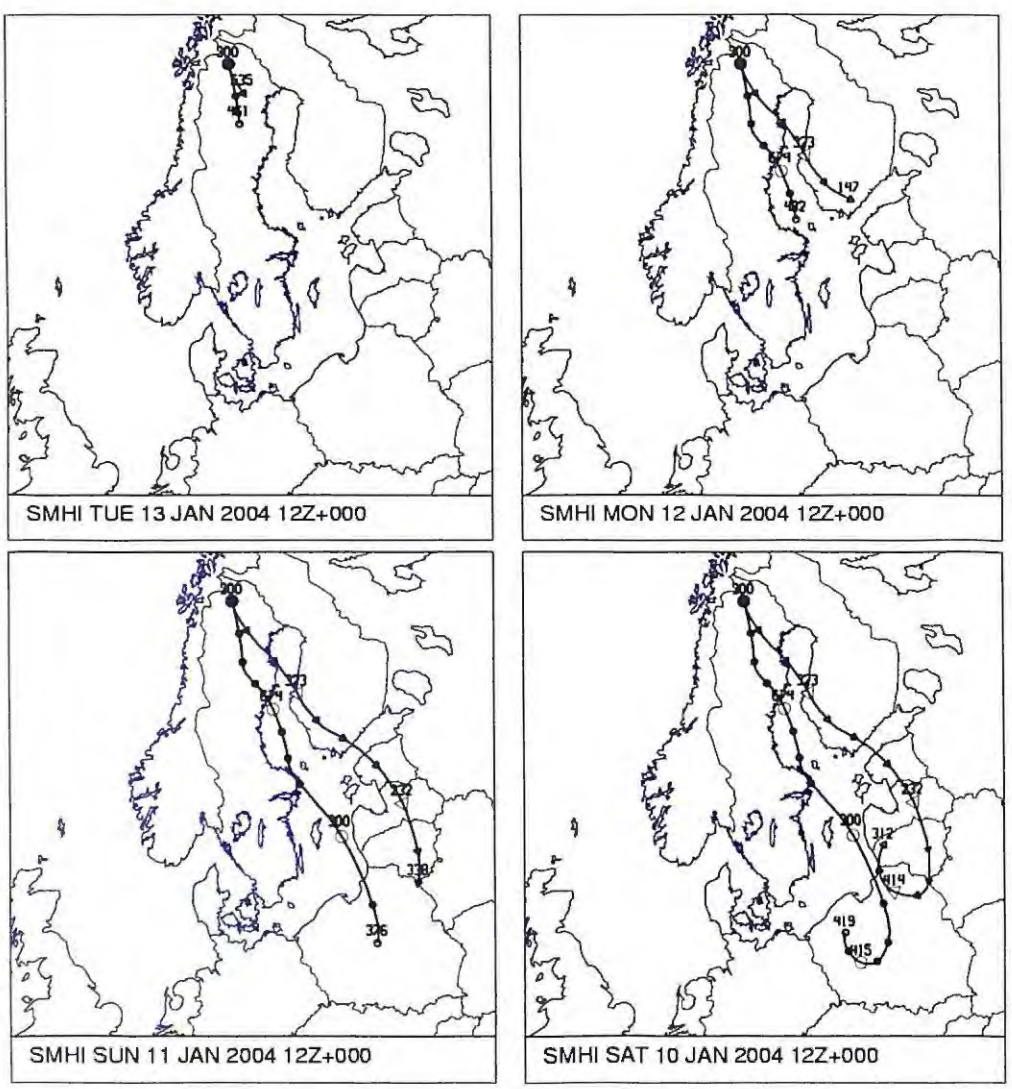

Figure 20: *The same as Figure 19 but only for the trajectories. The black line with circles starts at 09-14:00 UTC and the blue line with triangles at 09-13:18 UTC.*

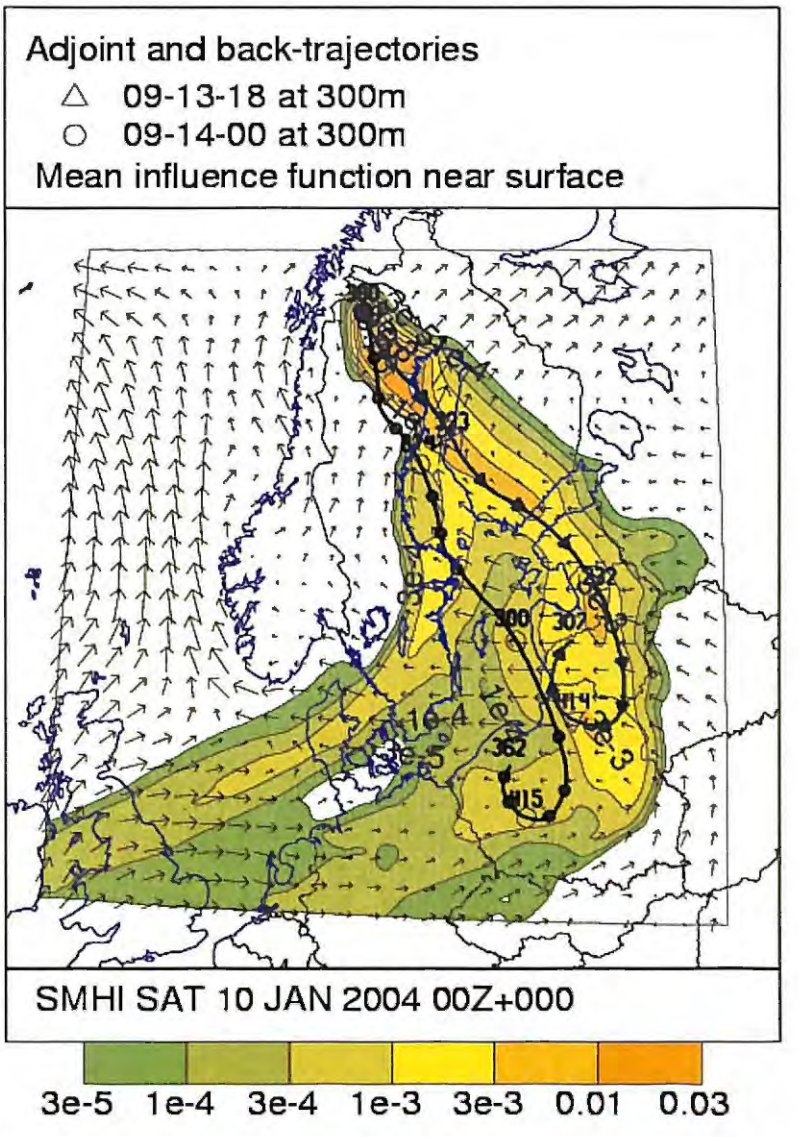

Figure 21: *Mean unit response influence function for a 6 hour response at Kiruna and trajectories starting in both ends of the response period. The black line with circles starts at 09-14:00 UTC and the blue line with triangles at 09-13:18 UTC. Non dimensional unit.*

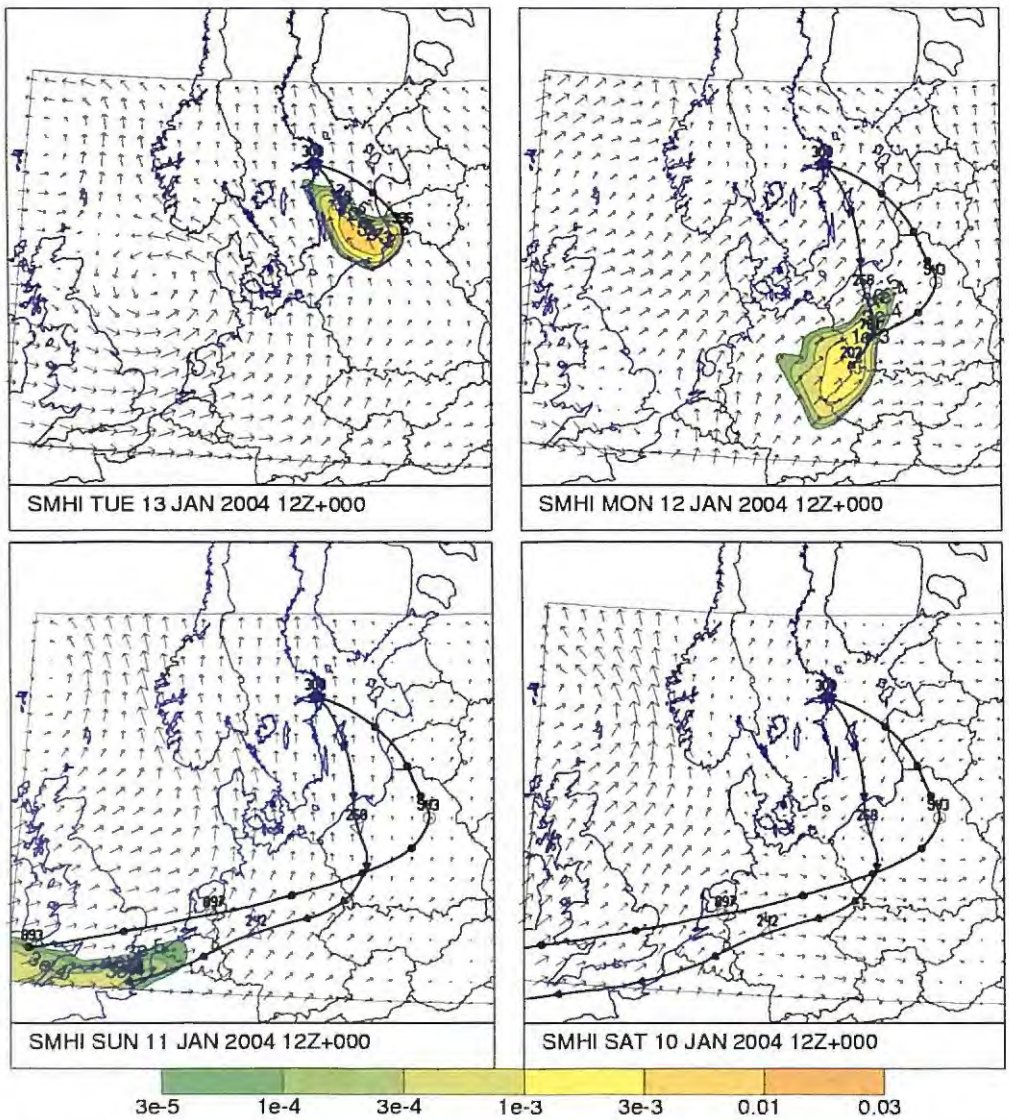

Figure 22: *Unit response influence function for a 6 hour response at Ursvik and trajectories starting in both ends of the response period. The black line with circles starts at 09-14:00 UTC and the blue line with triangles at 09-13:18 UTC. Non dimensional unit.*

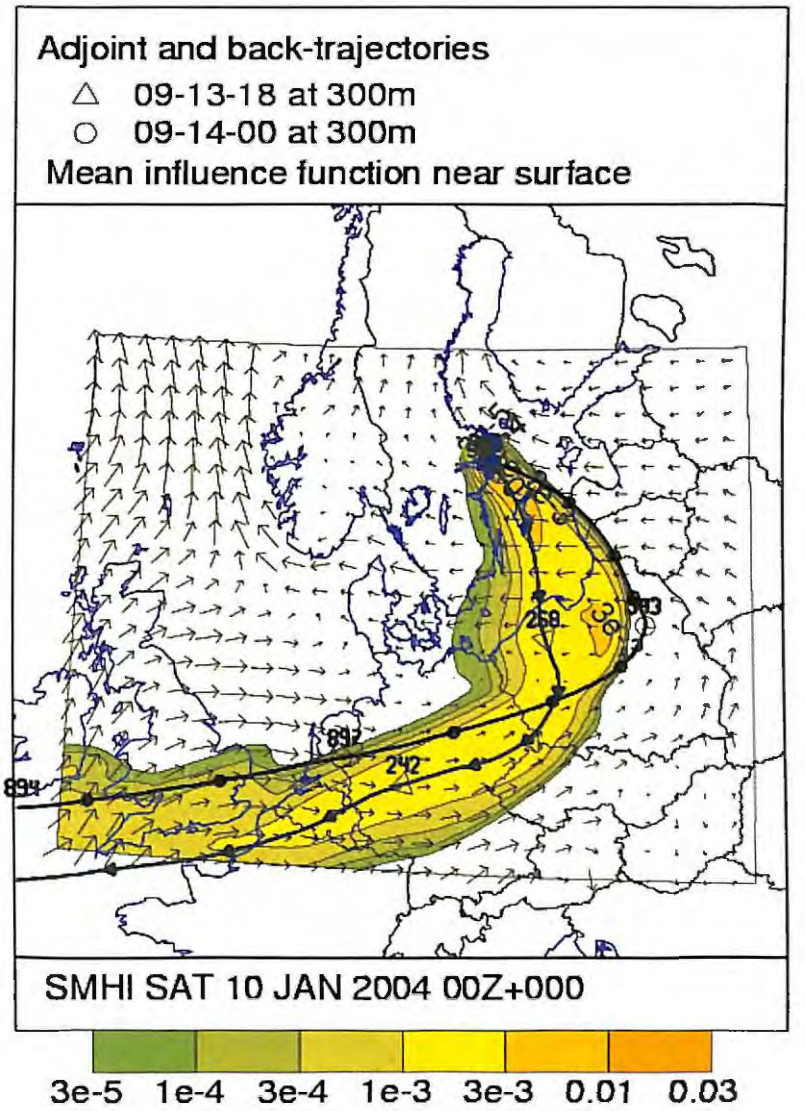

Figure 23: *Mean unit response influence function for a 6 hour response at Ursvik and trajectories starting in both ends of the response period. The black line with circles starts at 09-14:00 UTC and the blue line with triangles at 09-13:18 UTC. Non dimensional unit.*

8 Summary

We have shown that the adjoint technique using influence functions is rather similar to back-trajectories. The latter is in turn the most simple adjoint model, however, limited by its oversimplification of atmospheric transport. With the adjoint technique, applied to a 3D dispersion model, more of the atmospheric physics is accounted for. The adjoint technique also offers a mechanism for taking longer response times into account, or directly feed back observations for indication of the most possible source areas.

By some examples from e.g. the Chernobyl accident and the ETEX experiment we have gained confidence in the potential for the adjoint technique when observations are at hand, where the proper source areas have been accurately pointed out by the adjoint influence functions.

Back-trajectories have the advantage of being simple but may at the same time be misleading. In an operational environment the so called unit response approach would bring forward more detailed information about the possible source areas than traditional back-trajectories are able to provide, especially for longer time-integrations.

The deposition processes have not been included in this study. This is an acceptable limitation as long as the main objective is the influence area as such, and thus possible source areas, rather than a precise deduction of emission rates.

Acknowledgements

This research was funded by the Swedish Radiation protection agency (SSI) contract SSI P 1240.00.

References

Chardigny, E., Mose, R., Ackerer, P., Siegel, P., Mehreb, F. (1996) Groundwater flow parameter identification using a downscaling parameterization: a case study. Calibration and reliability in groundwater modelling., Kovar, Karel and van der Heijde, Paul (eds.), Wallingford, UK, IAHS (International Association of Hydrological Sciences) Press, 1996. pp. 137-145.

Courtier, P., Derber, J., Errico, R., Louis, J-F., and Vukisevic, T. (1993) Important literature on the use of the adjoint, variational methods and the Kalman filter in meteorology. *Tellus*, **45A**, 342-357.

Daescu, D, Sandu, A, Carmichael, G. (2003a) Direct and adjoint sensitivity analysis of chemical kinetic systems with KPP: Part I–theory and software tools. *Atmos. Environ.*, Vol. **37**, no. 36, pp. 5097-5114.

Daescu, D, Sandu, A, Carmichael, G. (2003b) Direct and adjoint sensitivity analysis of chemical kinetic systems with KPP: II–numerical validation and applications. *Atmos. Environ.*, Vol. **37**, no. 36, pp. 5097-5114.

Derber, J.C. (1989) A Variational Continuous Assimilation Technique. *Mon. Weath. Rev.*, **117**, pp. 2437-2446.

Elbern, H. and Schmidt, H. (1999) A four-dimensional variational chemistry data assimilation scheme for Eulerian chemistry transport modeling. *J. Geophysical Research*, Vol. **104**, No. D15, pp. 18,583-18,598.

Ghil, M. and Malanotte-Rizzoli, P. (1991) Data assimilation in Meteorology and Oceanography. *Adv. in Geophysics*, **33**, 141-266.

Houweling, S., Kaminski, T., Dentener, F., Lelieveld, J., Heimann, M- (1999) Inverse modeling of methane sources and sinks using the adjoint of a global transport model. *J. of Geophysical Research, Washington*, DC. Vol. **104**, no. D21, pp. 26137-26160. 1999

Konstadinos, P. and Robertson, L. (2003) Bayesian updating of atmospheric dispersion after a nuclear accident. *Applied Statistics* (in press).

Kontarev, G. (1980) Adjoint equation technique applied to meteorological problems. European Centre for Medium Range Weather Forecasts, Reading, Eng., Technical Report Sept., 1980. no. 21, 21 pp.

Le Dimet, F.-X., Navon, I. M., Daescu, D. N. (2002) Second-Order Information in Data Assimilation. *Mon. Weather Rev.*. Vol. **130**, no. 3, pp. 629-648.

Lorenc, A. C. (1988) Practical approximation to optimal four-dimensional objective analysis. *Monthly Weather Review*, Boston. Vol. **116**, no. 3, pp. 730-745.

Marchuk, G. I., Penenko, V. V. (1980) Study of the sensitivity of discrete models of atmospheric and oceanic dynamics. Izvestiya, Academy of Sciences, U.S.S.R., Atmospheric and Oceanic Physics, Wash., D.C. Vol. **15**, no. 11, pp. 785-789.

Marchuk, G. I. (1986) Mathematical models in environmental problems. *Studies In Mathematics and Its Applications*, Vol. **16**. Springer, Berlin.

Marchuk, G. I. (1994) Adjoint equations and analysis of complex systems. *Mathematics and Its Applications*, Vol. **295**. Kluwer Academic Press, Dordrecht.

McRae, G. J., Goodin, W. R. and Sienfeld, J. H. (1982) Numerical solution of the atmospheric diffusion equation for chemical Reacting flows. *J. Comp. Physics*, 45, pp

1-42.

Menut, L. (2003) Adjoint modeling for atmospheric pollution process sensitivity at regional scale *J. Geophys. Res.* (D Atmos.). Vol. 108, no. D17.

Mu, M., and Wang, J. (2003) A Method for Adjoint Variational Data Assimilation with Physical 'On-Off' Processes. *J. Atmos. Sci.*. Vol. **60**, no. 16, pp. 2010-2018.

Nodop K., Connolly, R. and Girardi, F. (1997) The European Tracer Experiment - Experimental Results and Database. In *Proceedings from the ETEX symposium an long-range atmospheric transport, model verification and emergency response*, Vienna 1997, K. Nodop (ed.), EUR 17346, European Commission.

Park, S. K., and Zupanski, D. (2003) Four-dimensional variational data assimilation for mesoscale and storm-scale applications. *Meteorol. Atmos. Phys.*. Vol. **82**, no. 1-4, pp. 173-208.

Persson, C., Rodhe, H. and De Geer, L. E. (1987) The Chernobyl accident - A meteorological analysis of how radionuclides reached and were deposited in Sweden. *Ambio*, 16, pp. 20-31.

Pudykiewicz, J. A. (1998) Application of adjoint tracer transport equations for evaluating source parameters. *Atm. Environ.*, Vol. **32**, No. 17, pp.3039-3050.

Purser, R., Wu, W., Parrish, D., Roberts, N. (2003) Numerical Aspects of the Application of Recursive Filters to Variational Statistical Analysis. Part I: Spatially Homogeneous and Isotropic Gaussian Covariances. *Mon. Weather Rev.*. Vol. **131**, no. 8, pp. 1524-1535.

Rivin, G. S., and Voronina, P. V. (2001) Aerosol modelling: The estimation of influence areas on the given region using the climatic data. *J. Aerosol Sci.*. Vol. **32**, suppl. 1, pp. S733-S734.

Robertson, L. and Langner, J. (1998) Source function estimate by means of variational data assimilation applied to the ETEX-I tracer experiment. *Atmos. Environ.*, **32**, 4219-4225.

Robertson, L. and Persson, C. (1993) Attempts to apply four dimensional data assimilation of radiological data using the adjoint technique. *Rad. Prot. Dos.*, **50**, 333-337.

Robertson, L., Langner, J. and Engardt, M. (1999) An Eulerian limited area Atmospheric transport model. *J. Appl. Meteor.*, **38**, 190-210.

Shen, J., and Kuo, A. Y. (1999) Application of inverse method to calibrate estuarine eutrophication model. *Journal of Environmental Engineering*, New York, NY. Vol. **124**, no. 5, pp. 409-418.

Sirkes, Z., and Tziperman, E. (2001) Identifying a Damped Oscillatory Thermohaline Mode in a General Circulation Model Using an Adjoint Model. *J. Phys. Oceanogr.* Vol. *31*, no. 8, pp. 2297-2306.

Schmidt, H., and Martin, D. (2003) Adjoint sensitivity of episodic ozone in the Paris area to emissions on the continental scale. *J. Geophys. Res.* (D Atmos.). Vol. **108**, no. D17.

Tanguay, M., and Polavarapu, S. (1999) The adjoint of the semi-Lagrangian treatment of the passive tracer equation. *Monthly Weather Review*, Boston, MA. Vol. **127**, no. 4, pp. 551-564.

Talagrand, O. and Courtier, P. (1987) Variational assimilation of meteorelogical observations with the adjoint vorticity equation. Part 1: Theory. *Q. J. R. Meteorol. Soc.*, **113**,

1311-1328.

Uliasz, M. (1987) Application of influence functions in numerical modelling of air pollution dispersion. Przeglad Geofizyczny, Warsaw. Vol. **32**, no. 1, pp. 3-19.

Uliasz, M. and Pielke, R. (1991) Application of the receptor oriented approach in mesoscale dispersion modeling. *Air Pollution Modeling and Its Application VIII*, H. van Dopt and D. G. Steyn (eds.), Plenum Press, New York, 399-407.

Uliasz, M., Pielke, R. A (1992) Receptor-oriented dispersion modeling: extension to nonlinear pollution chemistry. *Air pollution modeling and its application IX.*, van Dop, Han and Kallos, George (eds.), New York, NY, Plenum Press, 1992. pp. 171-178.

Van den Berghe, F. (1993) Variational assimilation of remote sensing data for the mapping of pollutant sources in lakes. Remote sensing for monitoring the changing environment of Europe., Winkler, Peter (ed.), Rotterdam, The Netherlands, A.A. Balkema, 1993. pp. 35-41.

Vogt, P. J., Pobanz, B. M., Alussi, F. J., Baskett, R. L. amd Sullivan T. J. (1998) ARAC simulation of the Algeciras, Spain steel mill CS-137 release. *Draft report*, Atmospheric Release Advisory Capability, Lawrence Livermore National Laboratory, Livermore, California.

Wotawa, G., De Geer, L.-E., Denier, P., Kalinowski, M., Toivonen, H., D'Amours, R., Desiato, F., Issartel, J.-P., Langer, M., Seibert, P., Frank, A., Sloan, C., Yamazawa, H. (2003) Atmospheric transport modelling in support of CTBT verification–overview and basic concepts. *Atmos. Environ.*. Vol. **37**, no. 18, pp. 2529-2537.

SMHIs publications

SMHI publishes six report series. Three of these, the R-series, are intended for international readers and are in most cases written in English. For the others the Swedish language is used.

Names of the Series	**Published since**
RMK (Report Meteorology and Climatology)	1974
RH (Report Hydrology)	1990
RO (Report Oceanography)	1986
METEOROLOGI	1985
HYDROLOGI	1985
OCEANOGRAFI	1985

Earlier issues published in serie RMK

1 Thompson, T., Udin, I., and Omstedt, A. (1974)
Sea surface temperatures in waters surrounding Sweden.

2 Bodin, S. (1974)
Development on an unsteady atmospheric boundary layer model.

3 Moen, L. (1975)
A multi-level quasi-geostrophic model for short range weather predictions.

4 Holmström, I. (1976)
Optimization of atmospheric models.

5 Collins, W.G. (1976)
A parameterization model for calculation of vertical fluxes of momentum due to terrain induced gravity waves.

6 Nyberg, A. (1976)
On transport of sulphur over the North Atlantic.

7 Lundqvist, J.-E., and Udin, I. (1977)
Ice accretion on ships with special emphasis on Baltic conditions.

8 Eriksson, B. (1977)
Den dagliga och årliga variationen av temperatur, fuktighet och vindhastighet vid några orter i Sverige.

9 Holmström, I., and Stokes, J. (1978)
Statistical forecasting of sea level changes in the Baltic.

10 Omstedt, A., and Sahlberg, J. (1978)
Some results from a joint Swedish-Finnish sea ice experiment, March, 1977.

11 Haag, T. (1978)
Byggnadsindustrins väderberoende, seminarieuppsats i företagsekonomi, B-nivå.

12 Eriksson, B. (1978)
Vegetationsperioden i Sverige beräknad från temperaturobservationer.

13 Bodin, S. (1979)
En numerisk prognosmodell för det atmosfäriska gränsskiktet, grundad på den turbulenta energiekvationen.

14 Eriksson, B. (1979)
Temperaturfluktuationer under senaste 100 åren.

15 Udin, I., och Mattisson, I. (1979)
Havsis- och snöinformation ur datorbearbetade satellitdata - en modellstudie.

16 Eriksson, B. (1979)
Statistisk analys av nederbördsdata. Del I. Arealnederbörd.

17 Eriksson, B. (1980)
Statistisk analys av nederbördsdata. Del II. Frekvensanalys av månadsnederbörd.

18 Eriksson, B. (1980)
Årsmedelvärden (1931-60) av nederbörd, avdunstning och avrinning.

19 Omstedt, A. (1980)
A sensitivity analysis of steady, free floating ice.

20 Persson, C., och Omstedt, G. (1980)
En modell för beräkning av luftföroreningars spridning och deposition på mesoskala.

21 Jansson, D. (1980)
Studier av temperaturinversioner och vertikal vindskjuvning vid Sundsvall-Härnösands flygplats.

22 Sahlberg, J., and Törnevik, H. (1980)
A study of large scale cooling in the Bay of Bothnia.

23 Ericson, K., and Hårsmar, P.-O. (1980)
Boundary layer measurements at Klock-rike. Oct. 1977.

24 Bringfelt, B. (1980)
A comparison of forest evapotranspiration determined by some independent methods.

25 Bodin, S., and Fredriksson, U. (1980)
Uncertainty in wind forecasting for wind power networks.

26 Eriksson, B. (1980)
Graddagsstatistik för Sverige.

27 Eriksson, B.(1981)
Statistisk analys av nederbördsdata. Del III. 200-åriga nederbördsserier.

28 Eriksson, B. (1981)
Den "potentiella" evapotranspirationen i Sverige.

29 Pershagen, H. (1981)
Maximisnödjup i Sverige (perioden 1905-70).

30 Lönnqvist, O. (1981)
Nederbördsstatistik med praktiska tillämpningar.
(Precipitation statistics with practical applications.)

31 Melgarejo, J.W. (1981)
Similarity theory and resistance laws for the atmospheric boundary layer.

32 Liljas, E. (1981)
Analys av moln och nederbörd genom automatisk klassning av AVHRR-data.

33 Ericson, K. (1982)
Atmospheric boundary layer field experiment in Sweden 1980, GOTEX II, part I.

34 Schoeffler, P. (1982)
Dissipation, dispersion and stability of numerical schemes for advection and diffusion.

35 Undén, P. (1982)
The Swedish Limited Area Model. Part A. Formulation.

36 Bringfelt, B. (1982)
A forest evapotranspiration model using synoptic data.

37 Omstedt, G. (1982)
Spridning av luftförorening från skorsten i konvektiva gränsskikt.

38 Törnevik, H. (1982)
An aerobiological model for operational forecasts of pollen concentration in the air.

39 Eriksson, B. (1982)
Data rörande Sveriges temperaturklimat.

40 Omstedt, G. (1984)
An operational air pollution model using routine meteorological data.

41 Persson, C., and Funkquist, L. (1984)
Local scale plume model for nitrogen oxides. Model description.

42 Gollvik, S. (1984)

Estimation of orographic precipitation by dynamical interpretation of synoptic model data.

43 Lönnqvist, O. (1984)
Congression - A fast regression technique with a great number of functions of all predictors.

44 Laurin, S. (1984)
Population exposure to SO and NO_x from different sources in Stockholm.

45 Svensson, J. (1985)
Remote sensing of atmospheric tempera-ture profiles by TIROS Operational Vertical Sounder.

46 Eriksson, B. (1986)
Nederbörds- och humiditetsklimat i Sverige under vegetationsperioden.

47 Taesler, R. (1986)
Köldperioden av olika längd och förekomst.

48 Wu Zengmao (1986)
Numerical study of lake-land breeze over Lake Vättern, Sweden.

49 Wu Zengmao (1986)
Numerical analysis of initialization procedure in a two-dimensional lake breeze model.

50 Persson, C. (1986)
Local scale plume model for nitrogen oxides. Verification.

51 Melgarejo, J.W. (1986)
An analytical model of the boundary layer above sloping terrain with an application to observations in Antarctica.

52 Bringfelt, B. (1986)
Test of a forest evapotranspiration model.

53 Josefsson, W. (1986)
Solar ultraviolet radiation in Sweden.

54 Dahlström, B. (1986)
Determination of areal precipitation for the Baltic Sea.

55 Persson, C. (SMHI), Rodhe, H. (MISU), De Geer, L.-E. (FOA) (1986)
The Chernobyl accident - A meteorological analysis of how radionucleides reached Sweden.

56 Persson, C., Robertson, L. (SMHI), Grennfelt, P., Kindbom, K., Lövblad, G., och Svanberg, P.-A. (IVL) (1987)
Luftföroreningsepisoden över södra Sverige 2 - 4 februari 1987.

57 Omstedt, G. (1988)
An operational air pollution model.

58 Alexandersson, H., Eriksson, B. (1989)
Climate fluctuations in Sweden 1860 - 1987.

59 Eriksson, B. (1989)
Snödjupsförhållanden i Sverige - Säsongerna 1950/51 - 1979/80.

60 Omstedt, G., Szegö, J. (1990)
Människors exponering för luftföroreningar.

61 Mueller, L., Robertson, L., Andersson, E., Gustafsson, N. (1990)
Meso-γ scale objective analysis of near surface temperature, humidity and wind, and its application in air pollution modelling.

62 Andersson, T., Mattisson, I. (1991)
A field test of thermometer screens.

63 Alexandersson, H., Gollvik, S., Meuller, L. (1991)
An energy balance model for prediction of surface temperatures.

64 Alexandersson, H., Dahlström, B. (1992)
Future climate in the Nordic region - survey and synthesis for the next century.

65 Persson, C., Langner, J., Robertson, L. (1994)
Regional spridningsmodell för Göteborgs och Bohus, Hallands och Älvsborgs län. (A mesoscale air pollution dispersion model for the Swedish west-coast region. In Swedish with captions also in English.)

66 Karlsson, K.-G. (1994)
Satellite-estimated cloudiness from NOAA AVHRR data in the Nordic area during 1993.

67 Karlsson, K-G. (1996)

Cloud classifications with the SCANDIA model.

68 Persson, C., Ullerstig, A. (1996)
Model calculations of dispersion of lindane over Europe. Pilot study with comparisons to measurements around the Baltic Sea and the Kattegat.

69 Langner, J., Persson, C., Robertson, L., and Ullerstig, A. (1996)
Air pollution Assessment Study Using the MATCH Modelling System. Application to sulfur and nitrogen compounds over Sweden 1994.

70 Robertson, L., Langner, J., Engardt, M. (1996)
MATCH - Meso-scale Atmosperic Transport and Chemistry modelling system.

71 Josefsson, W. (1996)
Five years of solar UV-radiation monitoring in Sweden.

72 Persson, C., Ullerstig, A., Robertson, L., Kindbom, K., Sjöberg, K. (1996)
The Swedish Precipitation Chemistry Network. Studies in network design using the MATCH modelling system and statistical methods.

73 Robertson, L. (1996)
Modelling of anthropogenic sulfur deposition to the African and South American continents.

74 Josefsson, W. (1996)
Solar UV-radiation monitoring 1996.

75 Häggmark, L., Ivarsson, K.-I. (SMHI), Olofsson, P.-O. (Militära vädertjänsten). (1997)
MESAN - Mesoskalig analys.

76 Bringfelt, B, Backström, H, Kindell, S, Omstedt, G, Persson, C, Ullerstig, A. (1997)
Calculations of PM-10 concentrations in Swedish cities- Modelling of inhalable particles

77 Gollvik, S. (1997)
The Teleflood project, estimation of precipitation over drainage basins.

78 Persson, C., Ullerstig, A. (1997)
Regional luftmiljöanalys för Västmanlands län baserad på MATCH modell-beräkningar och mätdata - Analys av 1994 års data

79 Josefsson, W., Karlsson, J.-E. (1997)
Measurements of total ozone 1994-1996.

80 Rummukainen, M. (1997)
Methods for statistical downscaling of GCM simulations.

81 Persson, T. (1997)
Solar irradiance modelling using satellite retrieved cloudiness - A pilot study

82 Langner, J., Bergström, R. (SMHI) and Pleijel, K. (IVL) (1998)
European scale modelling of sulfur, oxidized nitrogen and photochemical oxidants. Model development and evaluation for the 1994 growing season.

83 Rummukainen, M., Räisänen, J., Ullerstig, A., Bringfelt, B., Hansson, U., Graham, P., Willén, U. (1998)
RCA - Rossby Centre regional Atmospheric climate model: model description and results from the first multi-year simulation.

84 Räisänen, J., Döscher, R. (1998)
Simulation of present-day climate in Northen Europé in the HadCM2 OAGCM.

85 Räisänen, J., Rummukainen, M., Ullerstig, A., Bringfelt, B., Ulf Hansson, U., Willén, U. (1999)
The First Rossby Centre Regional Climate Scenario - Dynamical Downscaling of CO_2-induced Climate Change in the HadCM2 GCM.

86 Rummukainen, Markku. (1999)
On the Climate Change debate

87 Räisänen, Jouni (2000)
CO_2-induced climate change in northern Europé: comparison of 12 CMIP2 experiments.

88 Engardt, Magnuz (2000)
Sulphur simulations for East Asia using the MATCH model with meteorological data from ECMWF.

89 Persson, Thomas (2000)
Measurements of Solar Radiation in Sweden

1983-1998

90 Daniel B. Michelson, Tage Andersson
Swedish Meteorological and Hydrological Institute (2000)
Jarmo Koistinen, Finnish Meteorological Institute
Christopher G. Collier, Telford Institute of Environmental Systems, University of Salford
Johann Riedl, German Weather Service
Jan Szturc, Instiute of Meteorology and Water Management
Uta Gjertsen, The Norwegian Meteorological Institute
Aage Nielsen, Danish Meteorological Institute
Søren Overgaard, Danish Meteorological Institute
BALTEX Radar Data Centre Products and their Methodologies

91 Josefsson, Weine (2000)
Measurements of total ozone 1997 – 1999

92 Andersson, Tage (2000)
Boundary clear air echos in southern Sweden

93 Andersson, Tage (2000)
Using the Sun to check some weather radar parameters

94 Rummukainen, M.,S. Bergström, E. Källén, L. Moen, J. Rodhe, M. Tjernström (2000)
SWECLIM – The First Three Years

95 Meier, H. E Markus (2001)
The first Rossby Centre regional climate scenario for the Baltic Sea using a 3D coupled ice-ocean model

96 Landelius, Tomas, Weine Josefsson, Thomas Persson (2001)
A system for modelling solar radiation parameters with mesoscale spatial resolution

97 Karlsson, Karl-Göran (2001)
A NOAA AVHRR cloud climatology over Scandinavia covering the period 1991-2000

98 Bringfelt, B., Räisänen, J., Gollvik, S., Lindström, G., Graham, P., Ullerstig, A., (2001)
The land surface treatment for the Rossby entre Regional Atmospheric Climate Model - version 2 (RCA2)

99 Kauker, Frank , Alfred Wegener Institute for Polar and Marine Research, Germany and Meier, H.E. Markus, Swedish Meteorological and Hydrological Institute, Rossby Centre, Sweden (2002)
Reconstructing atmospheric surface data for the period 1902-1998 to force a coupled ocean-sea ice model of the Baltic Sea.

100 Klein, Thomas., Bergström, Robert., Persson, Christer (2002)
Parameterization of dry deposition in MATCH

101 Räisänen, Jouni., Hansson U., Ullerstig A., Döscher R., Graham L P., Jones C., Meier M., Samuelsson P., Willén U (2003)
GCM driven simulations of recent and future climate with the Rossby Centre coupled atmosphere - Baltic Sea regional climate model RCAO

102 Tjernström, M., Rummukainen, M., Bergström, S., Rodhe, J., Persson, G., (2003)
Klimatmodellering och klimatscenarier ur SWECLIMs perspektiv.

103 Segersson, David (2003)
Numerical Quantification of Driving Rain on Buildings

104 Rummukainen, Markku and the SWECLIM participants (2003)
The Swedish regional climate modeling program 1996-2003. Final report.

SMHI

Swedish Meteorological and Hydrological Institute
SE-601 76 Norrköping Sweden
Tel +46 11 495 80 00 Fax +46 11 495 80 01

ISSN 0347-2116